Spectroscopy at nanometer scale

1. Spectroscopy vs. Microscopy
2. Physics of the spectroscopies
3. Spectroscopies for H and H_2
4. Experimental setups for the spectroscopies
5. Physics and Chemistry of nanomaterials

Microscopy is the science of investigating small objects that are too small for the naked eye. The microscopic study involves revelation of the structure and morphology of the matter under investigation.

Spectroscopy is the study of the interaction between matter and radiated energy. With the mechanism of "resonance", the characteristic nature of the matter can be probed.

Both microscopic and spectroscopic techniques are essential for nanoscience research.

Spectroscopy originates from the dispersion of light through a prism.

Prism

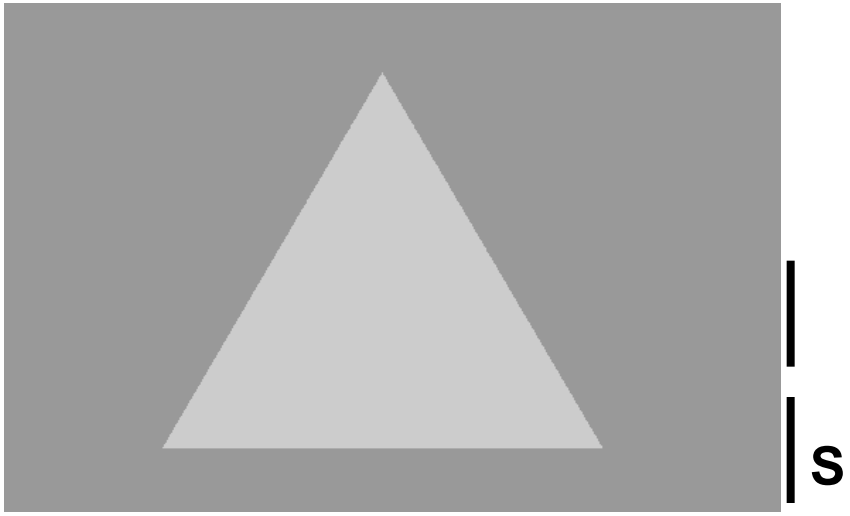

Grating

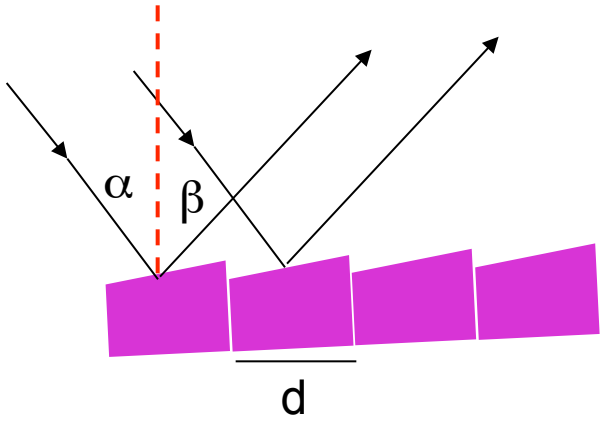

$\Delta s = d\,(\sin\alpha - \sin\beta)$
$= m\lambda$

Mechanical resonance

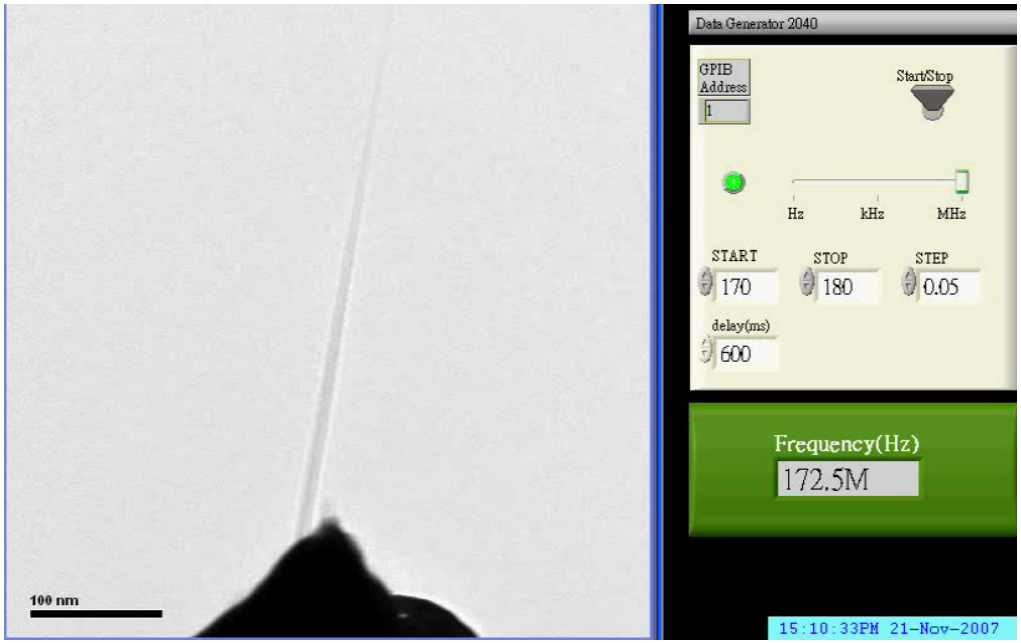

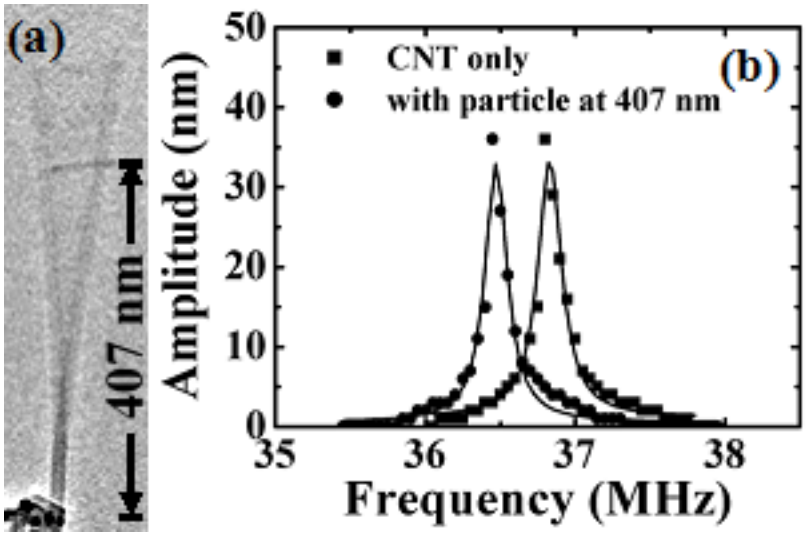

Absorption spectra of atomic hydrogen

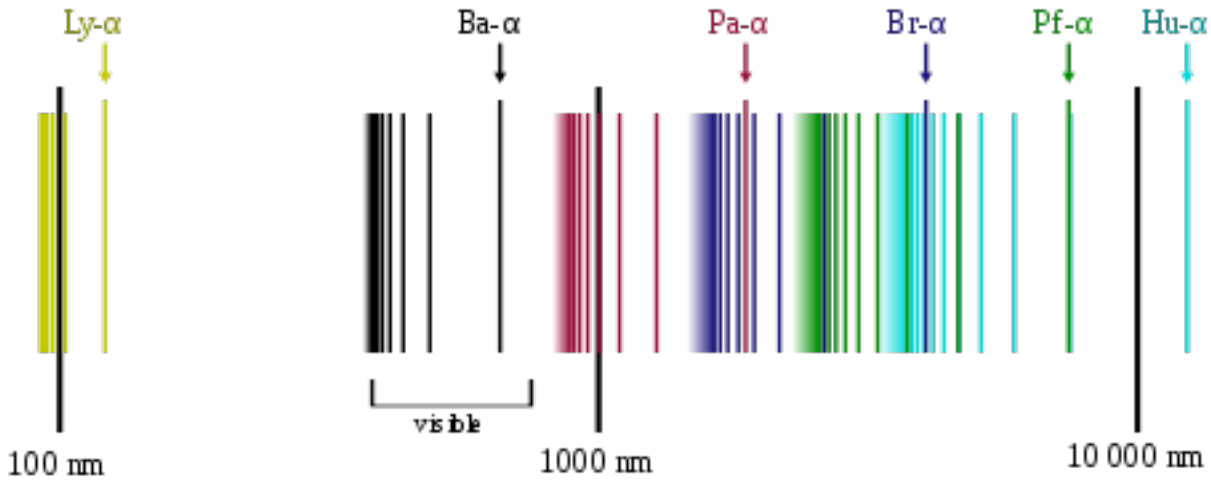

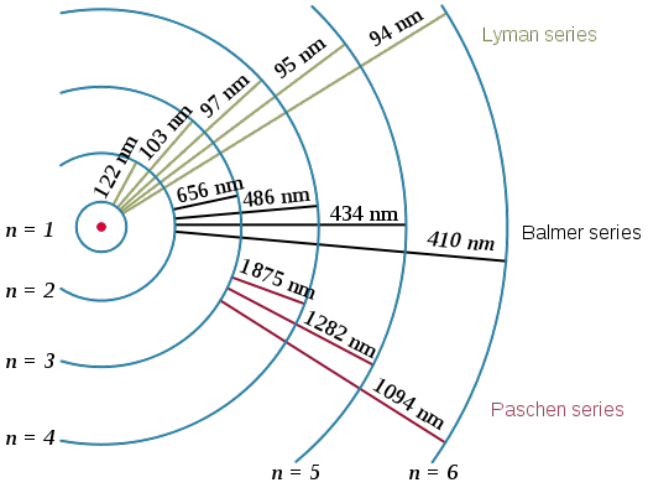

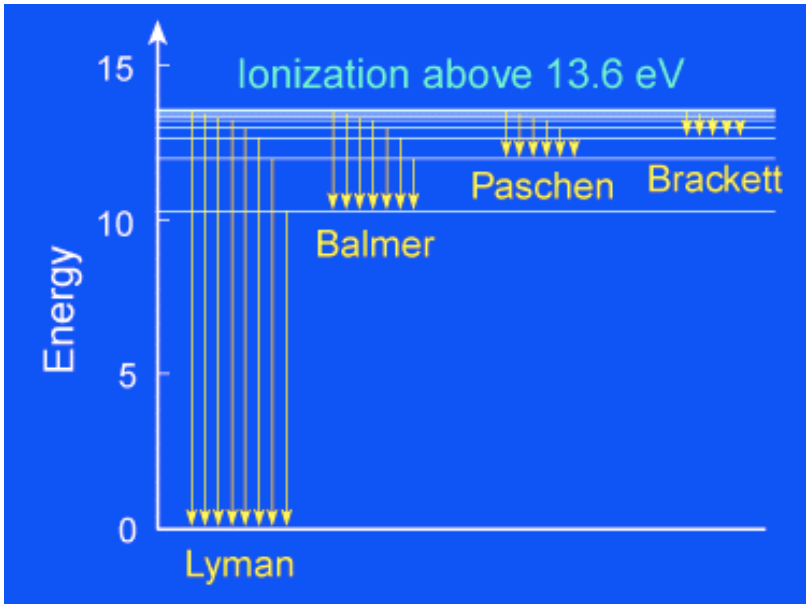

Bohr model of hydrogen atom

$$E = -\frac{Z^2 me^4}{8n^2h^2\varepsilon_0^2} = \frac{-13.6Z^2}{n^2}eV \qquad r = \frac{n^2h^2\varepsilon_0}{Z\pi me^2} = \frac{n^2a_0}{Z}$$

$$a_0 = 0.0529nm = Bohr\ radius$$

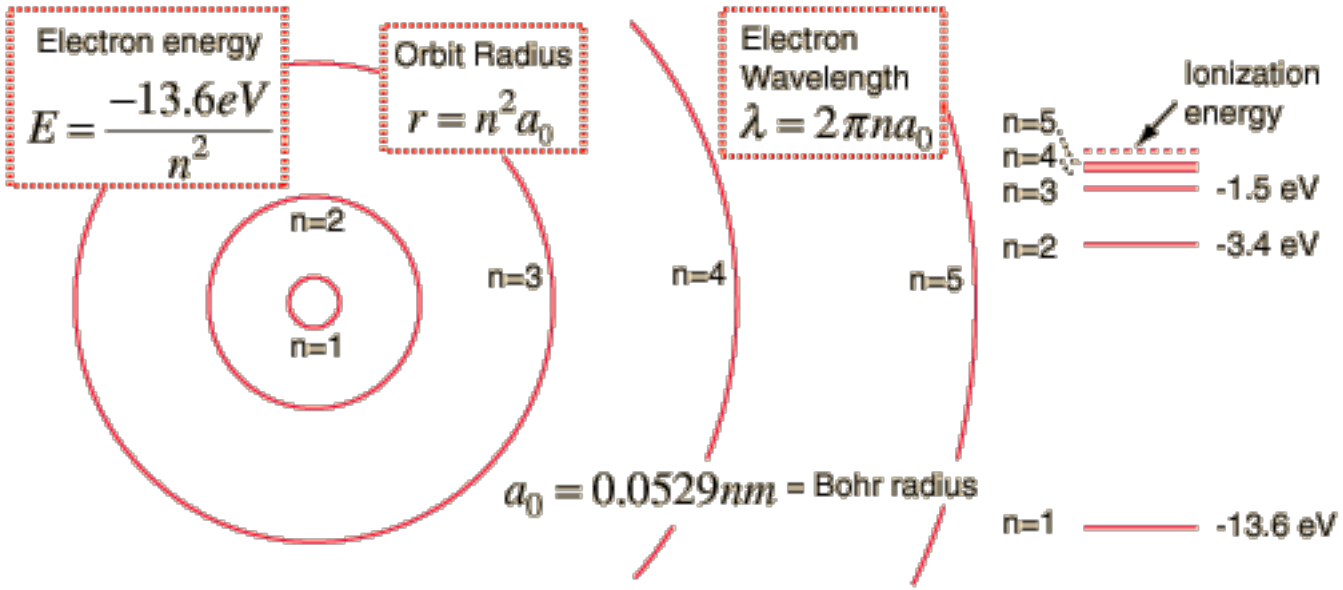

Electron Transitions

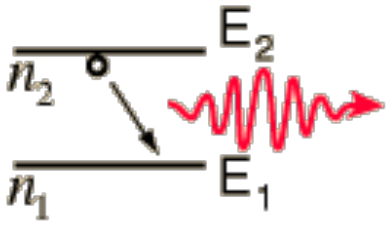

A downward transition involves emission of a photon of energy:

$$E_{photon} = h\upsilon = E_2 - E_1$$

Given the expression for the energies of the hydrogen electron states:

$$h\upsilon = \frac{2\pi^2 me^4}{h^2}\left[\frac{1}{n_1^2} - \frac{1}{n_2^2}\right] = -13.6\left[\frac{1}{n_1^2} - \frac{1}{n_2^2}\right] \text{eV}$$

Fermi's golden rule is a way to calculate the transition rate (probability of transition per unit time) between two eigenstates

$$T_{i\to f} = \frac{2\pi}{\hbar}\left|\langle f|H'|i\rangle\right|^2 \rho,$$

Absorption spectra of molecular hydrogen

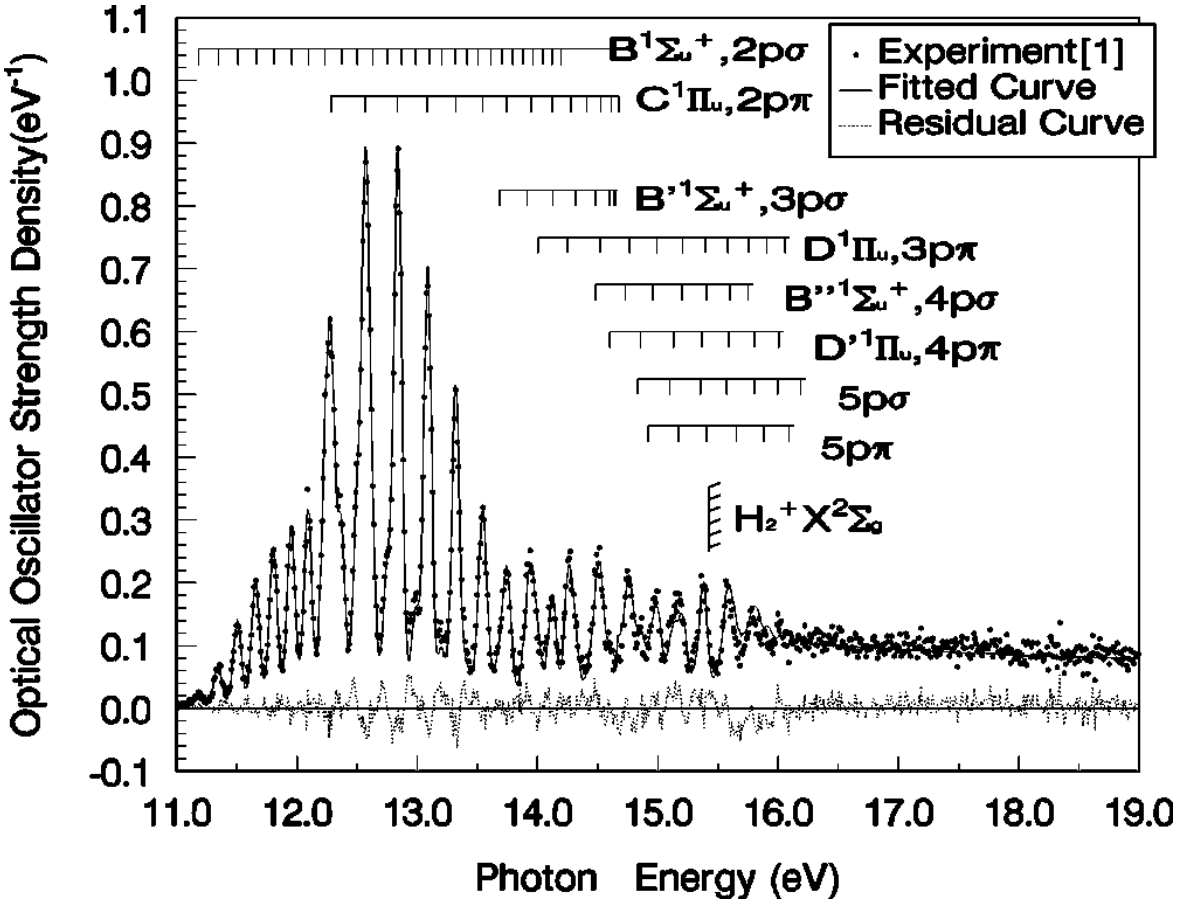

Zhi Ping Zhong et al., Phys. Rev. A **60**, 236 (1999)

Born-Oppenheimer Approximation

$$\psi_{\text{molecule}}(\vec{r}_i, \vec{R}_j) = \psi_{\text{electrons}}(\vec{r}_i, \vec{R}_j)\,\psi_{\text{nuclei}}(\vec{R}_j)$$

$m_e << m_n$

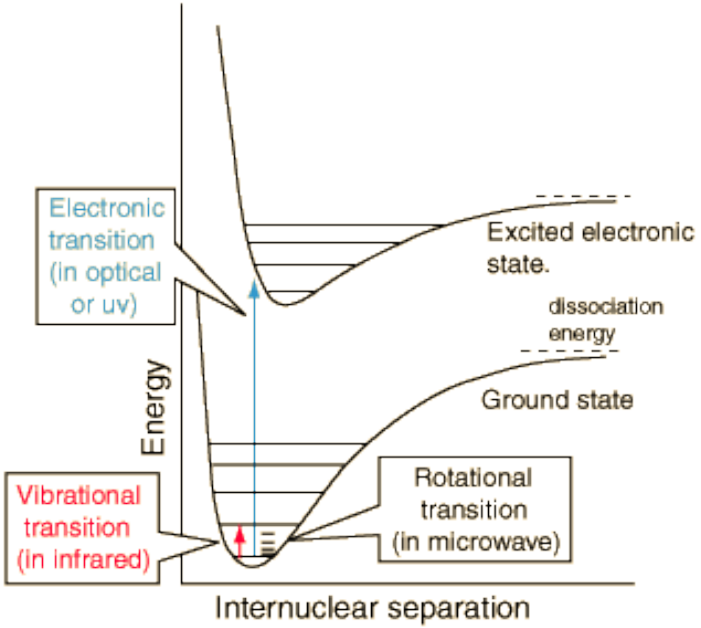

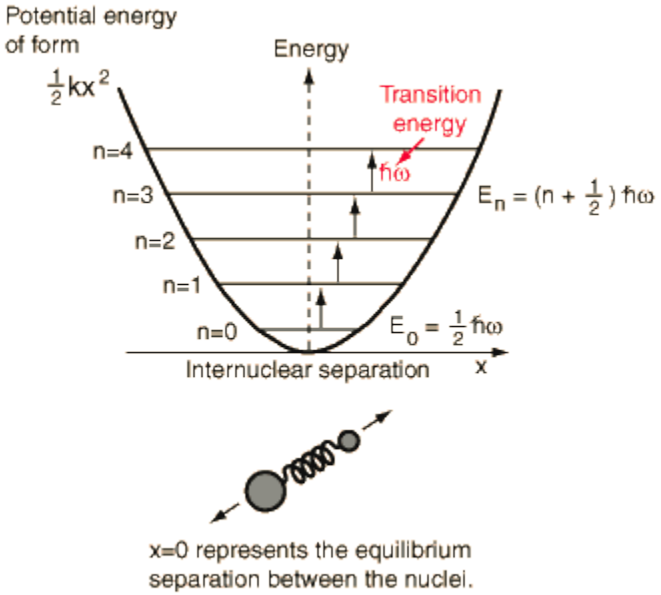

Various spectroscopic methods

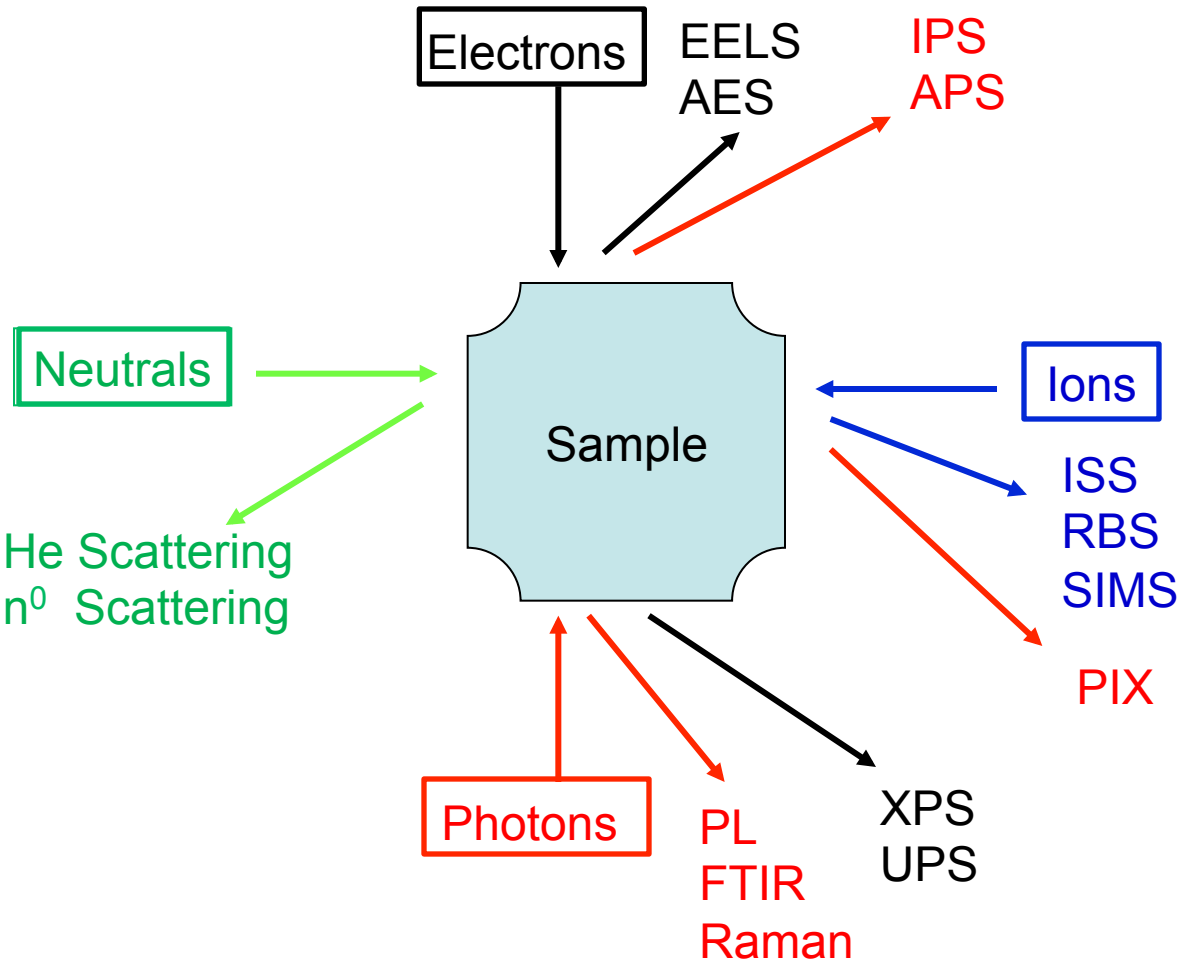

Electronic Spectroscopy

1. Photons in, photons out – PL
2. Photons in, electrons out – UPS, XPS
3. Electrons in, electrons out – EELS

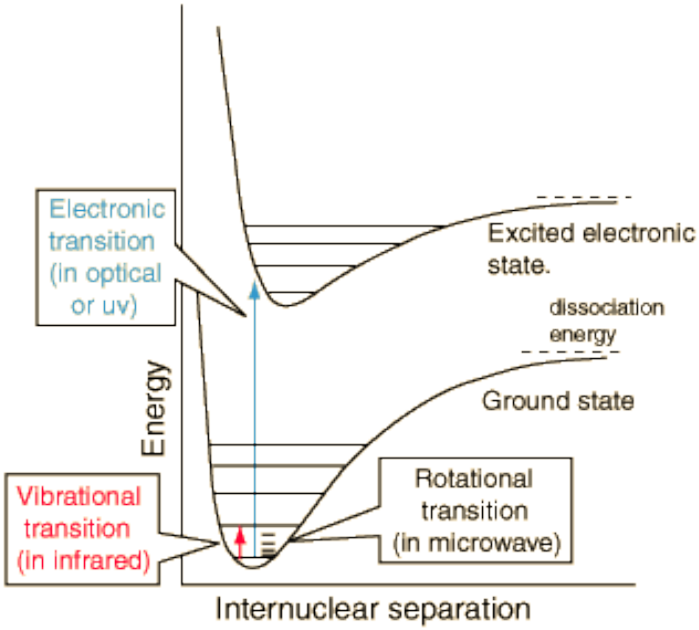

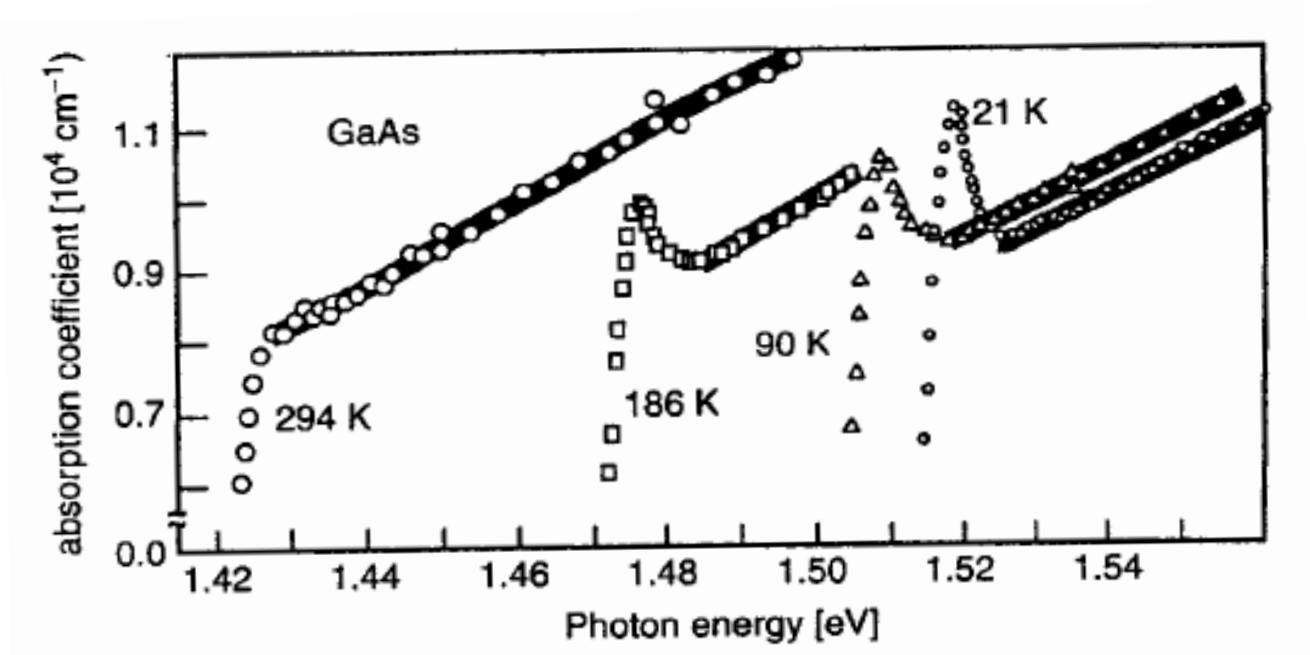

Binding energy and effective radius for the exciton

$E_e = (m^*/m_e)(\varepsilon/\varepsilon_0)^{-2}$ (13.6 eV)

$a_{eff} = (\varepsilon/\varepsilon_0)(m^*/m_e)^{-1}$ (0.0529 nm)

For GaAs, $\varepsilon/\varepsilon_0 \sim 13.2$ and $m^* \sim 0.067 m_e$

then $E_e \sim 5$ meV and $a_{eff} \sim 10$ nm

One dimensional size effect

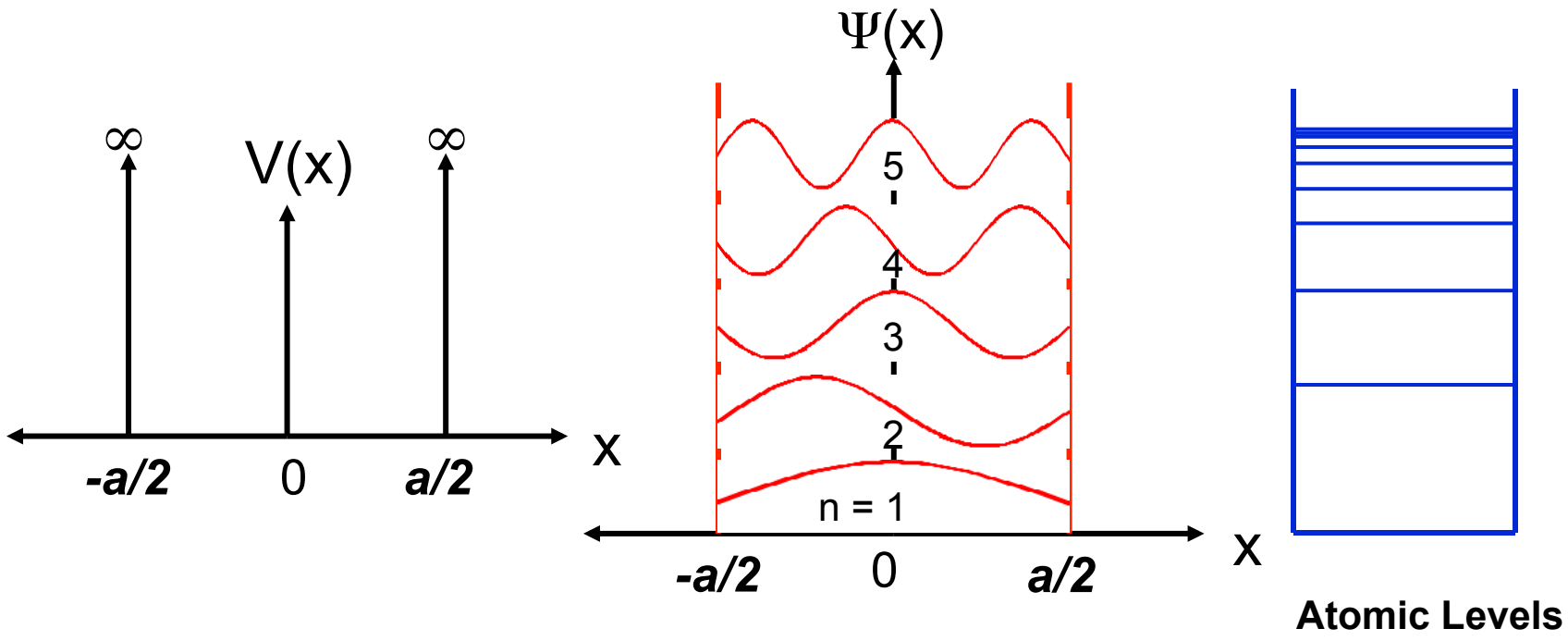

$$\Psi(x) = \begin{cases} \sin(n\pi x/a), & n \text{ even} \\ \cos(n\pi x/a), & n \text{ odd} \end{cases}$$

$$E = n^2\pi^2\hbar^2/2ma^2,\ n = 1,2,3\ldots$$

Size effect

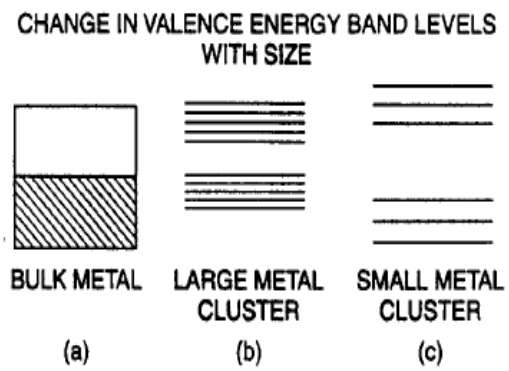
CHANGE IN VALENCE ENERGY BAND LEVELS WITH SIZE
BULK METAL
(a)
LARGE METAL CLUSTER
(b)
SMALL METAL CLUSTER
(c)

Size

Ratio of surface atoms

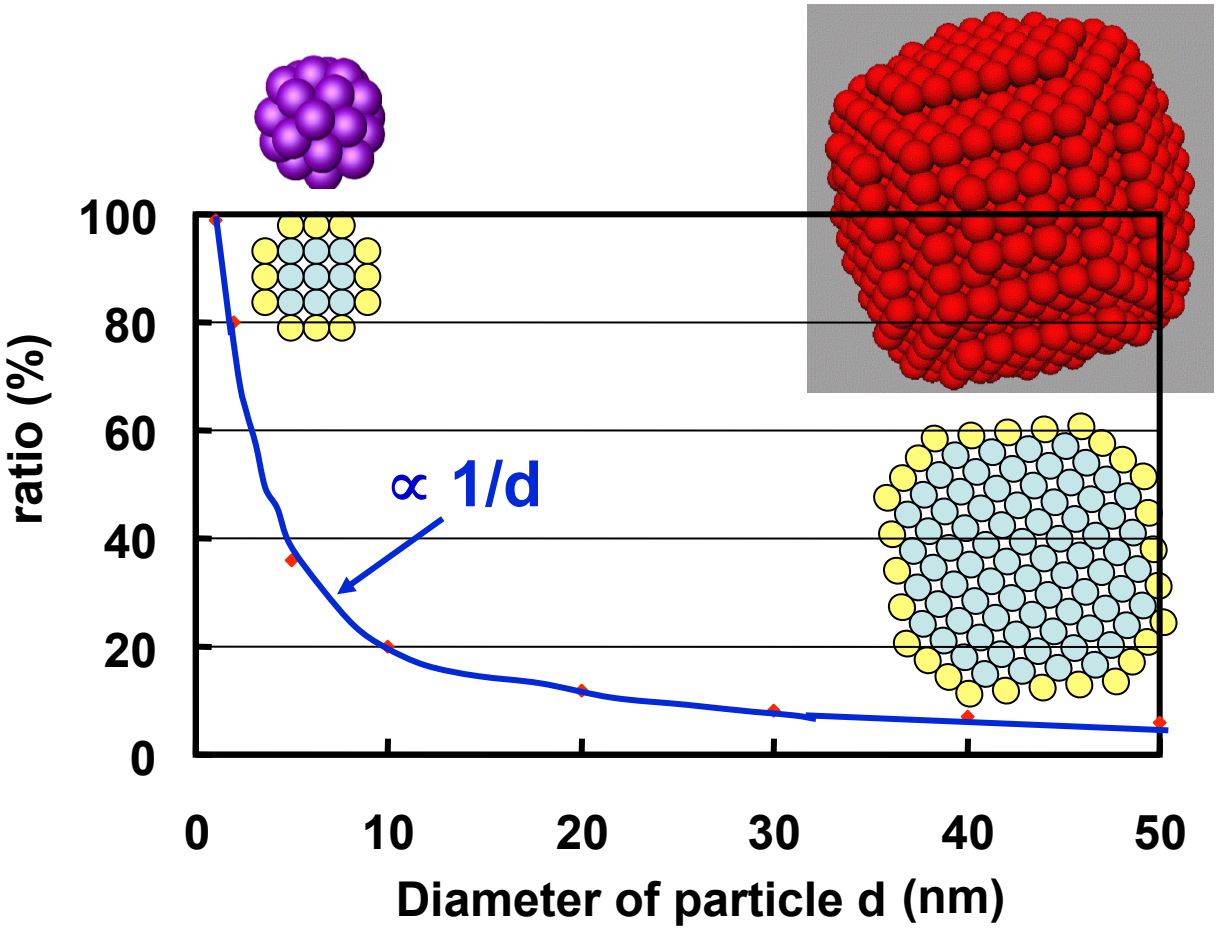

Au nanoparticle as an example

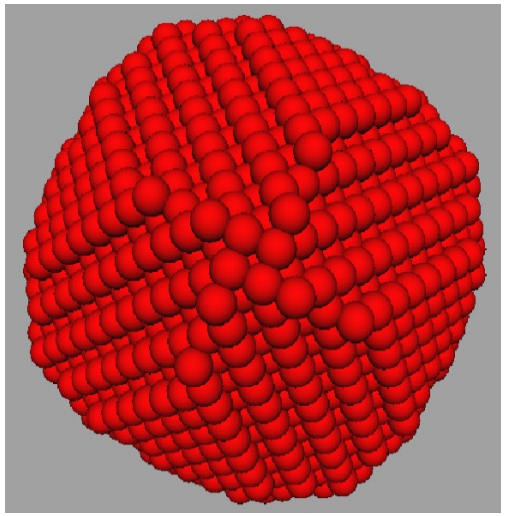

$$E_F = (\hbar^2/2m)\,(3\pi^2 n)^{2/3}$$

$$g(E_F) = (3/2)\,(n/E_F)$$

$$\delta = 2/[g(E_F)V] = (4/3)\,(E_F/N)$$

Number of valence electrons (N) contained in the particles is roughly 40,000. Assume the Fermi energy (E_F) is about 7 eV for Au, then

$$\delta \sim 0.22 \text{ meV} \sim 2.5 \text{ K}$$

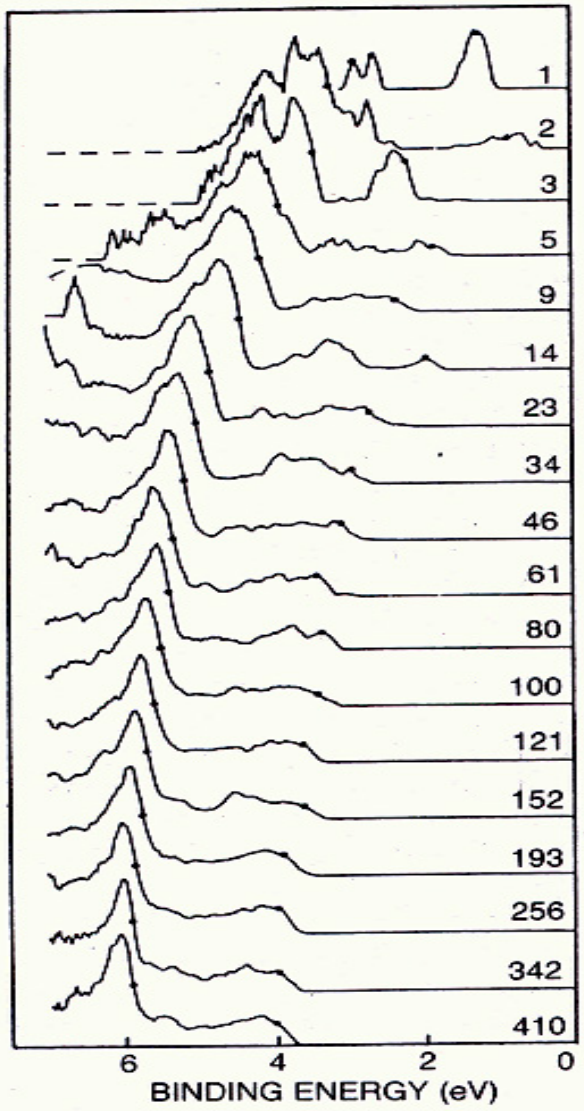

Ultraviolet photoemission spectra of ionized copper clusters Cu_N^- ranging in size from N of 1 to 410 show the energy distribution versus binding energy of photoemitted electrons. These photoemission patterns show the evolution of the 3d band of Cu as a function of cluster size. As the cluster size increases, the electron affinity approaches the value of the bulk metal work function. (Adapted from ref. 10.) **Figure 5**

Semiconductor quantum dots

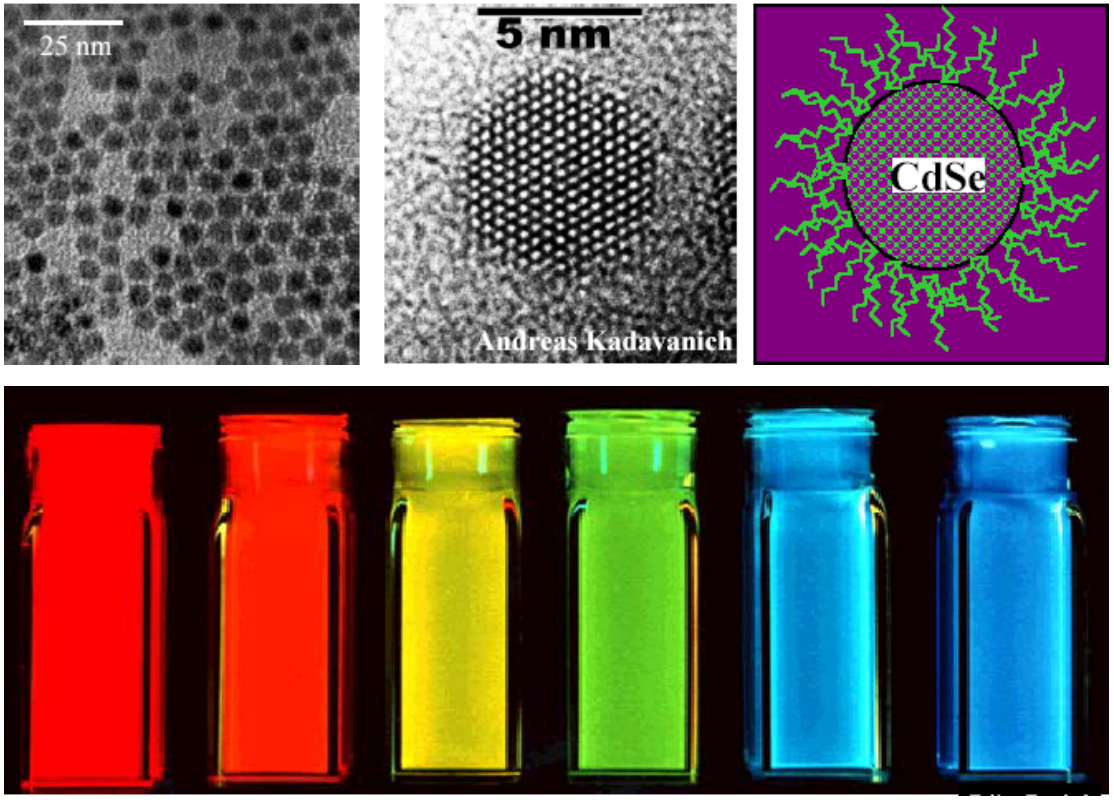

(Reproduced from Quantum Dot Co.)

Optical properties of nanoparticles (in the visible light range)

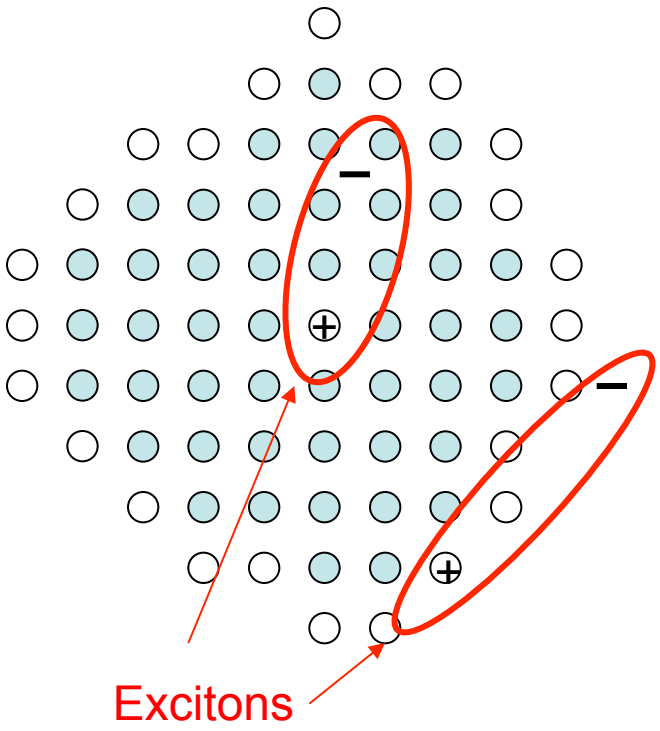

(1) Blue shift:
Due mainly to the energy-gap widening because of the size effect.

(2) Red shift:
Bond shortening resulted from surface tension causes more overlap between neighboring electron wavefunctions. Valence bands will be broadened and the gap becomes narrower.

(3) Enhanced exciton absorption:
Due mainly to the increased probability of exciton formation because of the confining effect.

Optical properties

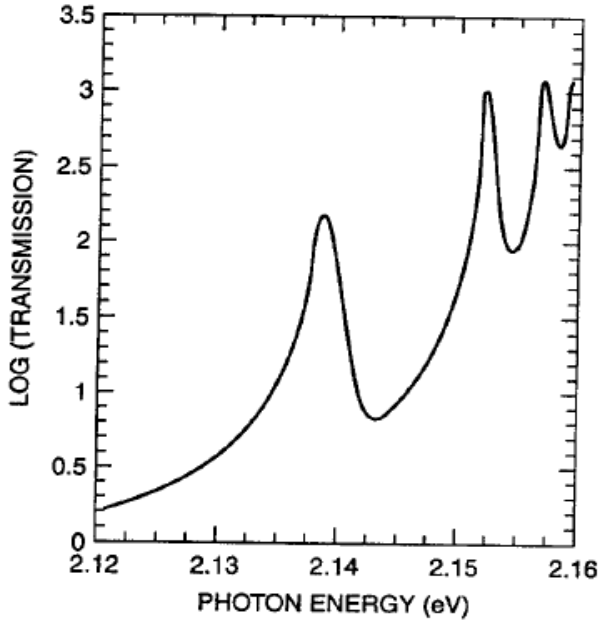

Figure 4.19. Optical absorption spectrum of hydrogen-like transitions of excitons in Cu_2O. [Adapted from P. W. Baumeister, *Phys. Rev.* **121**, 359 (1961).]

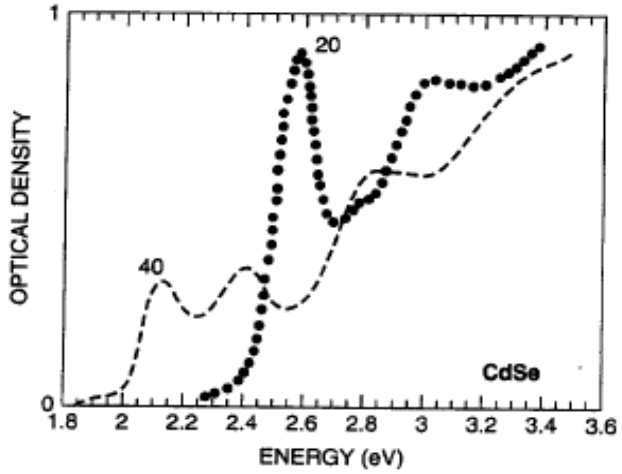

Figure 4.20. Optical absorption spectrum of CdSe for two nanoparticles having sizes 20 Å and 40 Å, respectively. [Adapted from D. M. Mittleman, *Phys. Rev.* **B49**, 14435 (1994).]

Scanning Tunneling Spectroscopy

1. Barrier Height Imaging

Up to now homogeneous surfaces were considered. If there is an inhomogeneous compound in the surface the work function will be inhomogeneous as well. This alters the local barrier height. Differentiation of tunneling current yields

$$\frac{d(\ln I)}{ds} \propto \sqrt{\Phi}$$

Thus the work function can directly be measured by varying the tip-sample distance, which can be done by modulating the current with the feedback turned on.

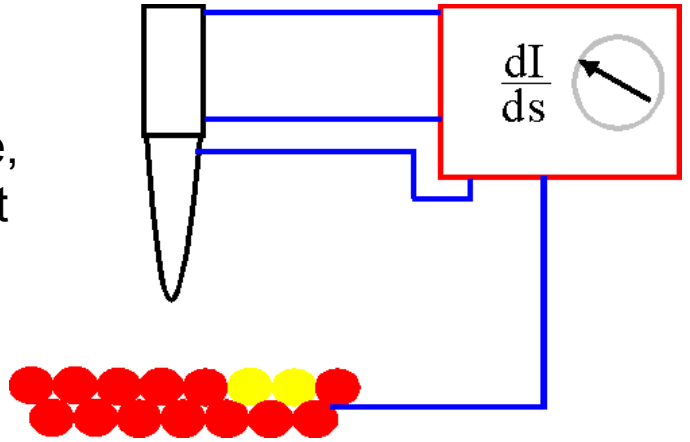

STM Images of Si(111)-(7×7)

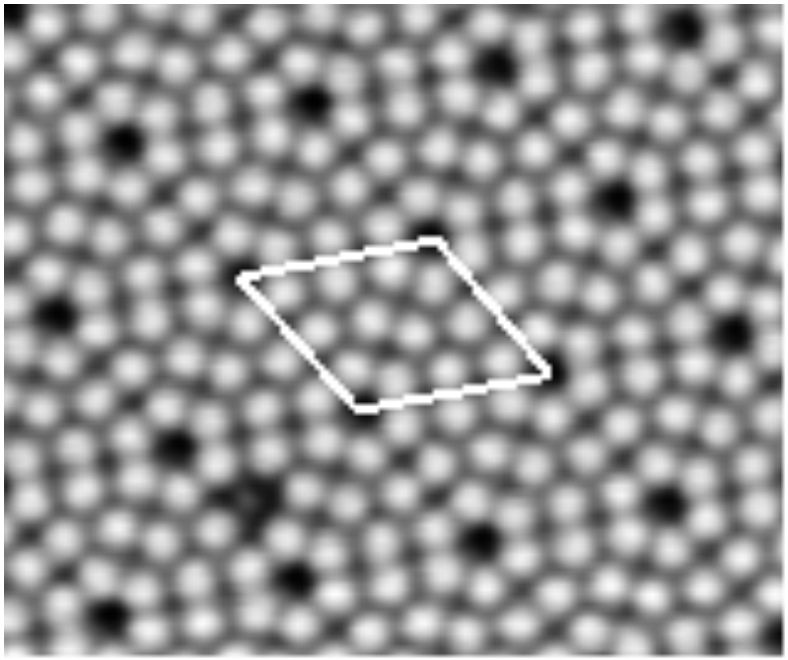

Empty-state image

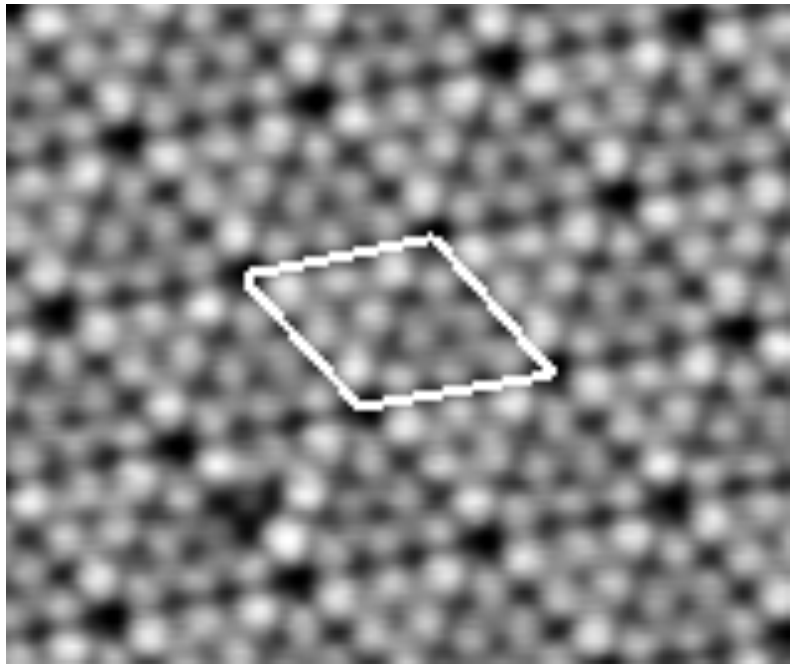

Filled-state image

Electronic Structures at Surfaces

Not Tunneling

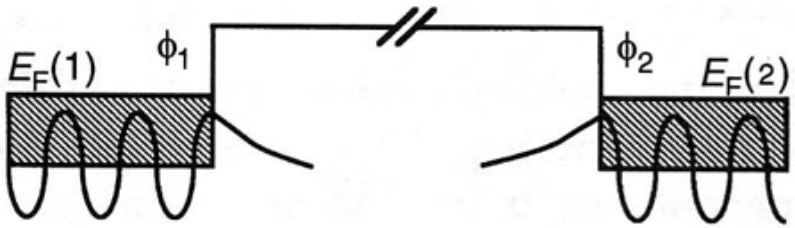

Empty-State Imaging

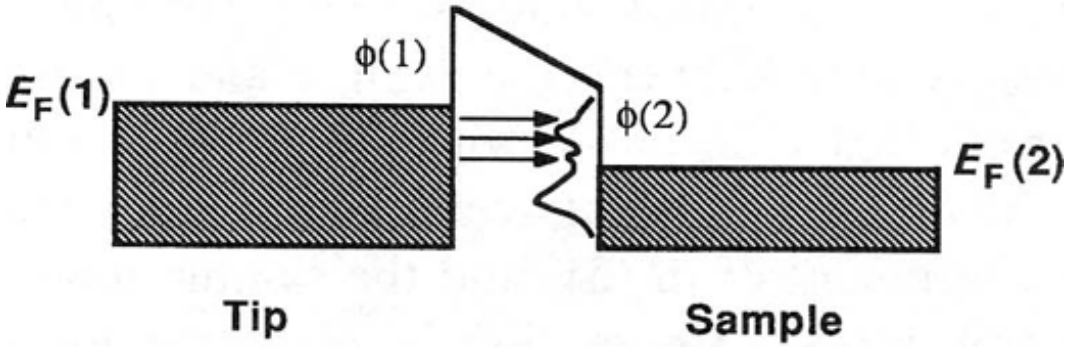

Tunneling

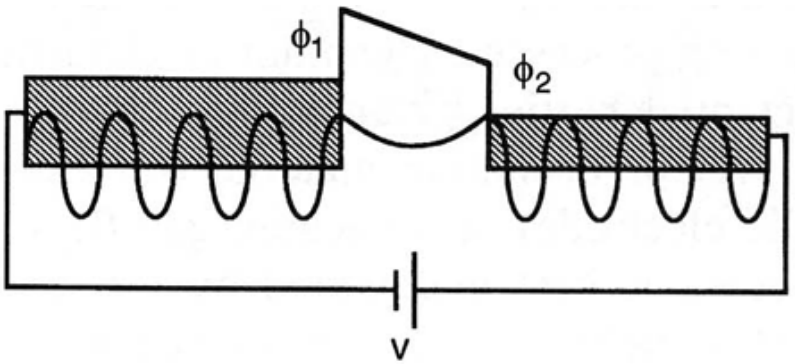

Filled-State Imaging

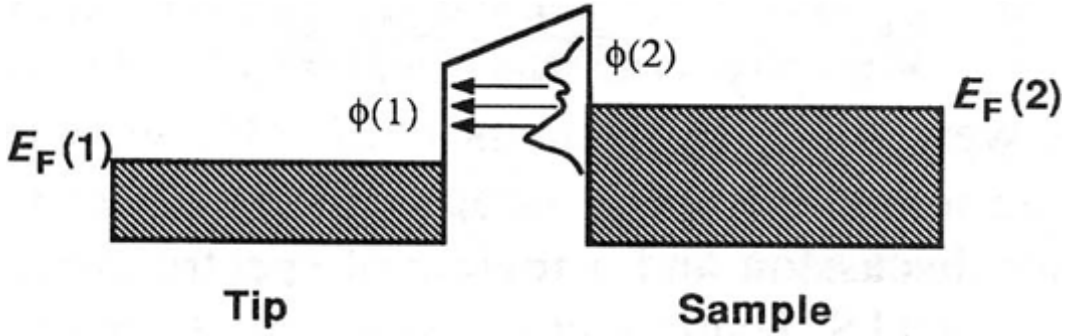

2. dI/dV imaging

If the matrix element and the density of states of the tip is nearly constant, the tunneling current can be estimated to

$$I \propto \int_0^{eV} \rho_{sa}\left(E_F - eV + \varepsilon\right) d\varepsilon$$

Differentiation yields the density of state

$$\frac{dI}{dV} \propto \rho_{sa}\left(E_F - eV\right)$$

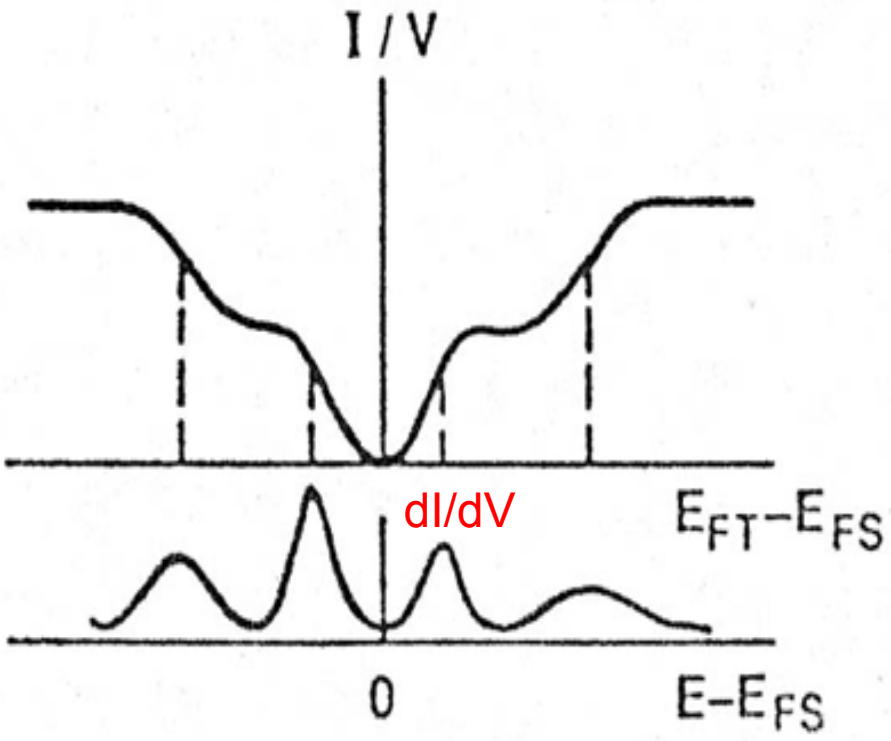

Density of state (DOS)

The mapping of surface density of states can be deduced by

- Modulation of the bias voltage (dI/dV imaging): The tip is scanned in the constant current mode to give a constant distance to the sample. A dither voltage of ~1k Hz is added to the bias voltage while the feedback loop remains active. A lock-in technique is employed to obtain the current change at the dither frequency.
- Current-Imaging Tunneling Spectroscopy (CITS): The tip is scanned in the constant current mode to give a constant distance to the sample. At each point the feedback loop is disabled and a current-voltage curve (I-V curve) is recorded.

STS of Si(111)-(7x7)

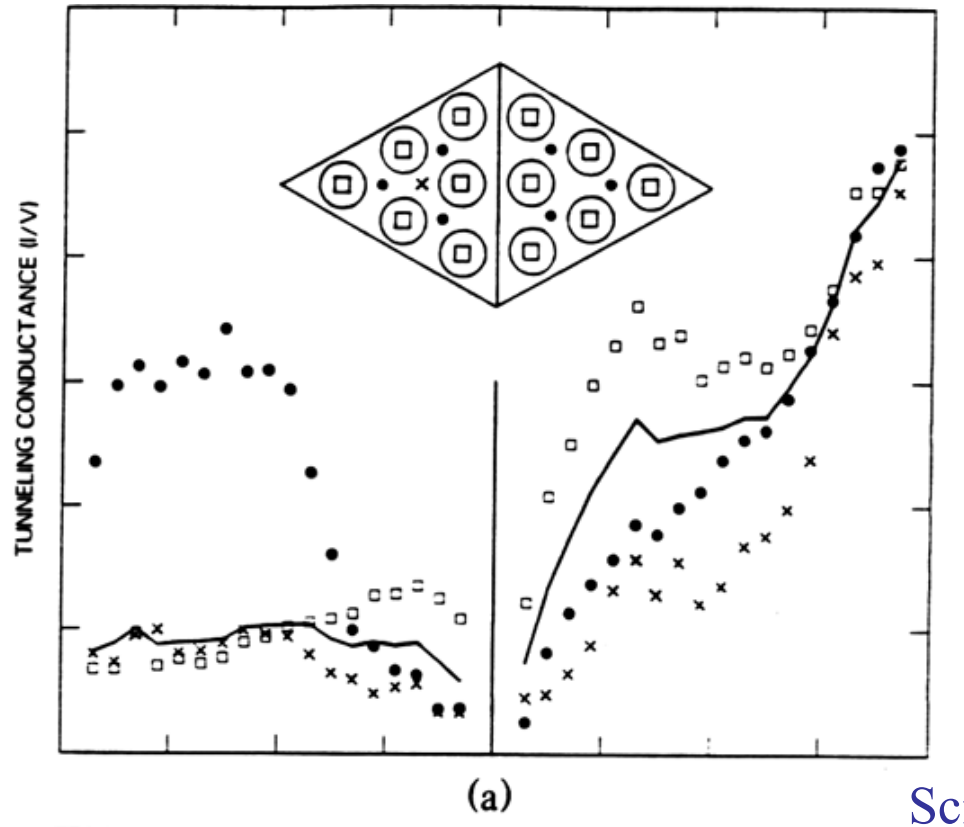

Science **234**, 304 (1986).

STS of Si(111)-(7x7)

topograph

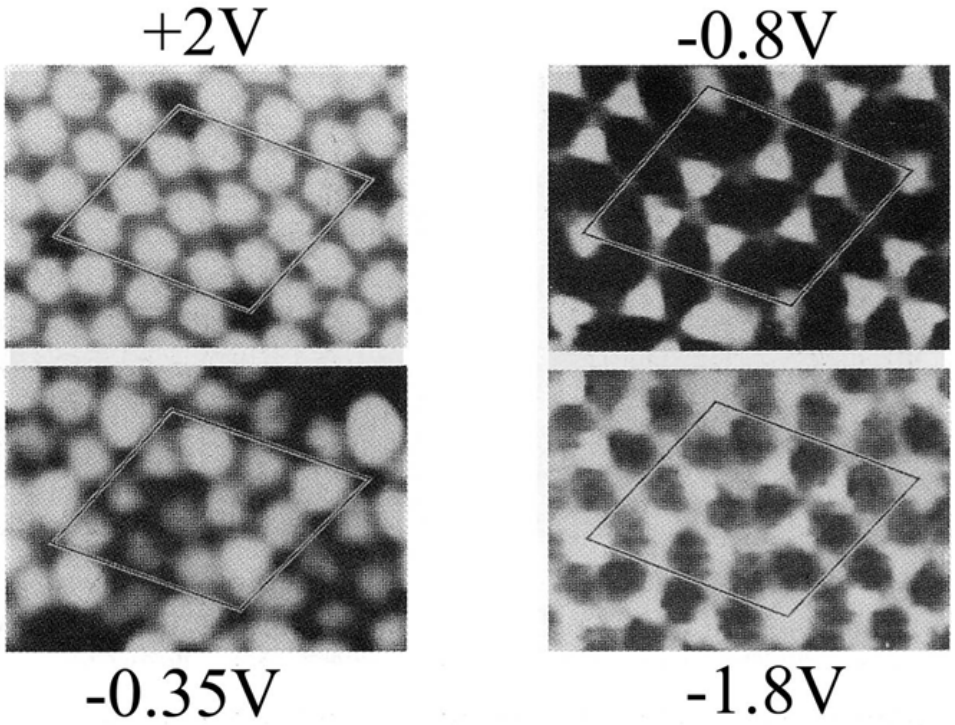

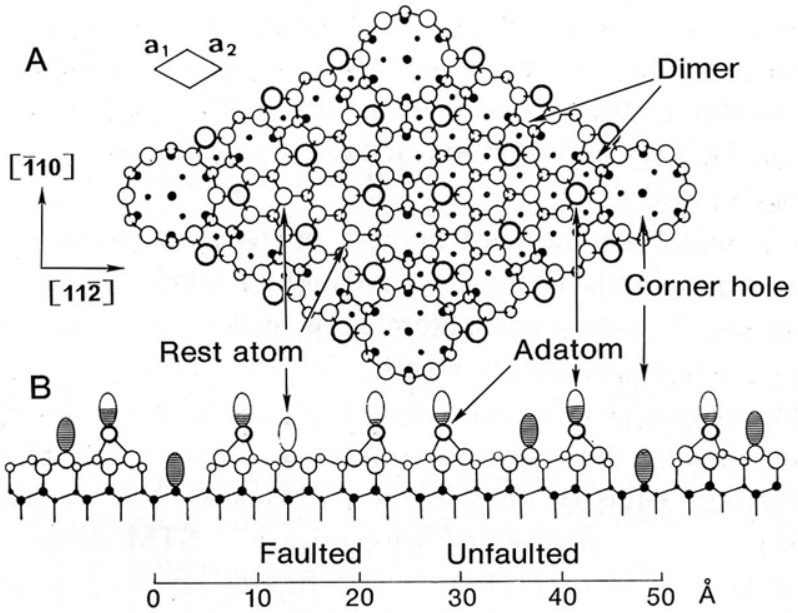

1. Science **234**, 304-309 (1986).
2. Phys. Rev. Lett. **56**, 1972-1975 (1986).

Density of states of various dimensions

3D

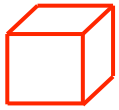

$D(\varepsilon) \sim \varepsilon^{1/2}$

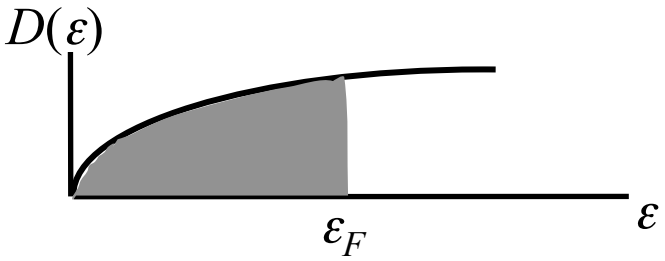

2D

$D(\varepsilon) = m^* / \pi\hbar^2$

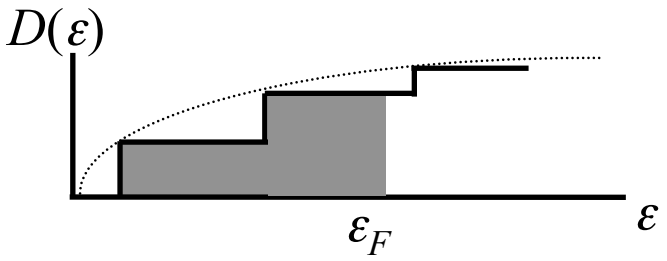

1D

$D(\varepsilon) \sim (\varepsilon - E_n)^{-1/2}$

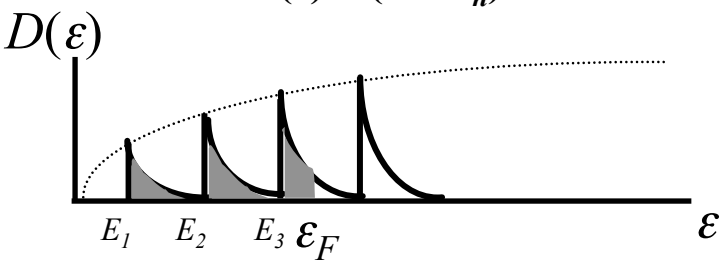

0D

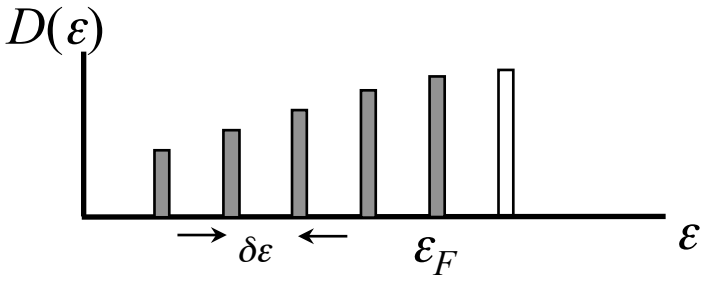

Electronic Structure of Single-wall Nanotubes

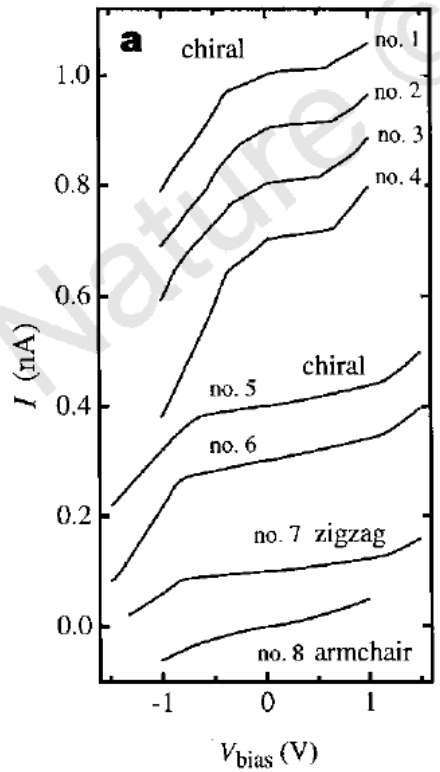

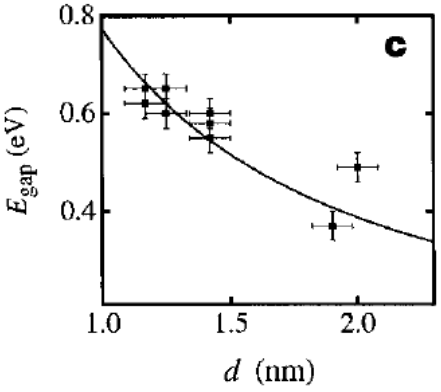

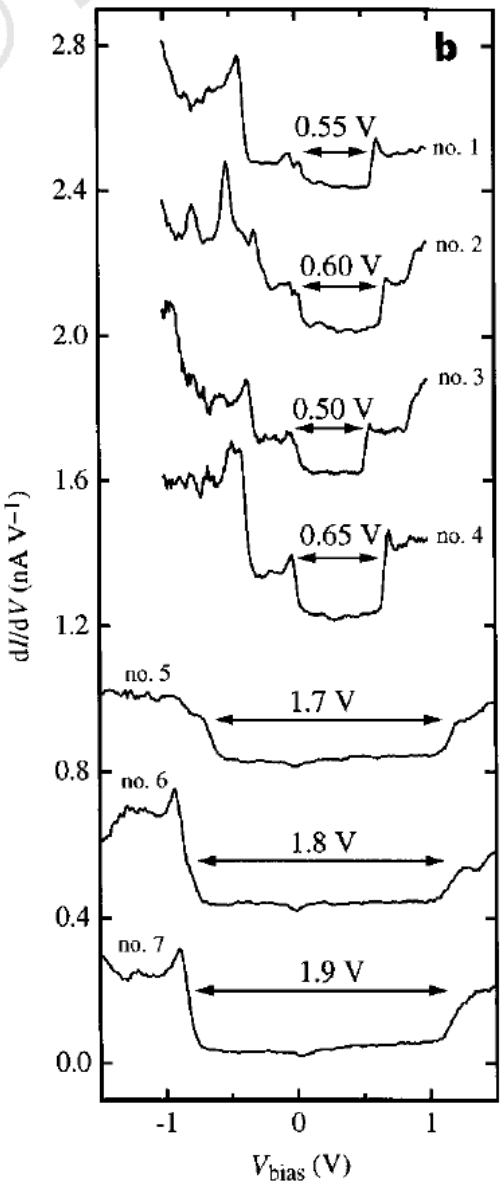

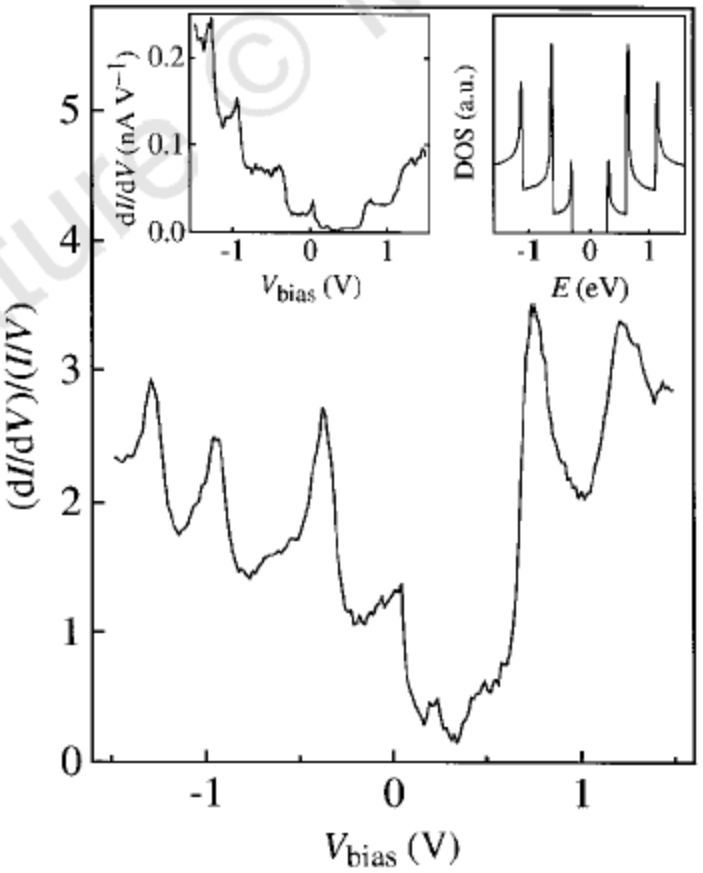

Nature **391**, 59 (1998).

Quantum size effect

λ = de Broglie wavelength of electron
a = thickness of metal film

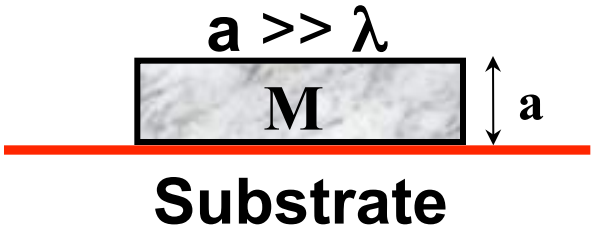

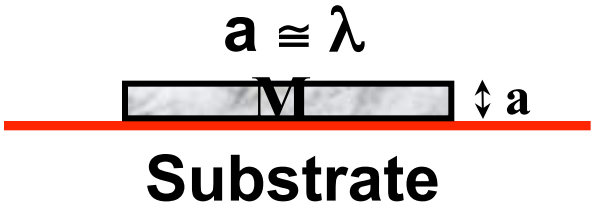

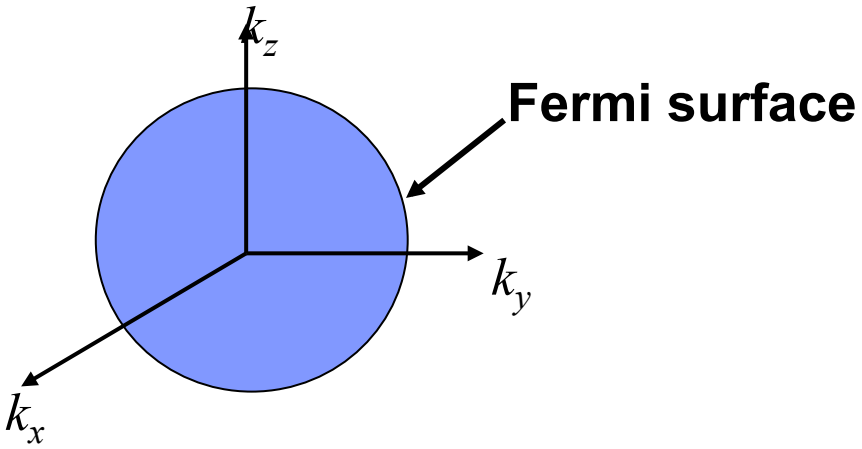

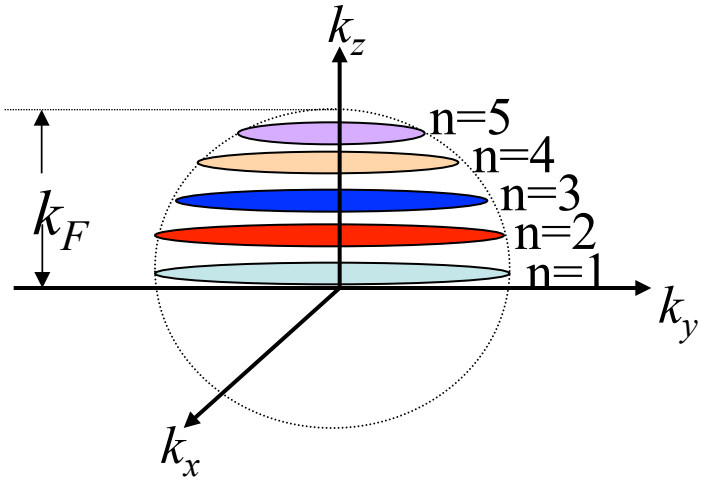

Pb islands on the IC Pb/Si(111)

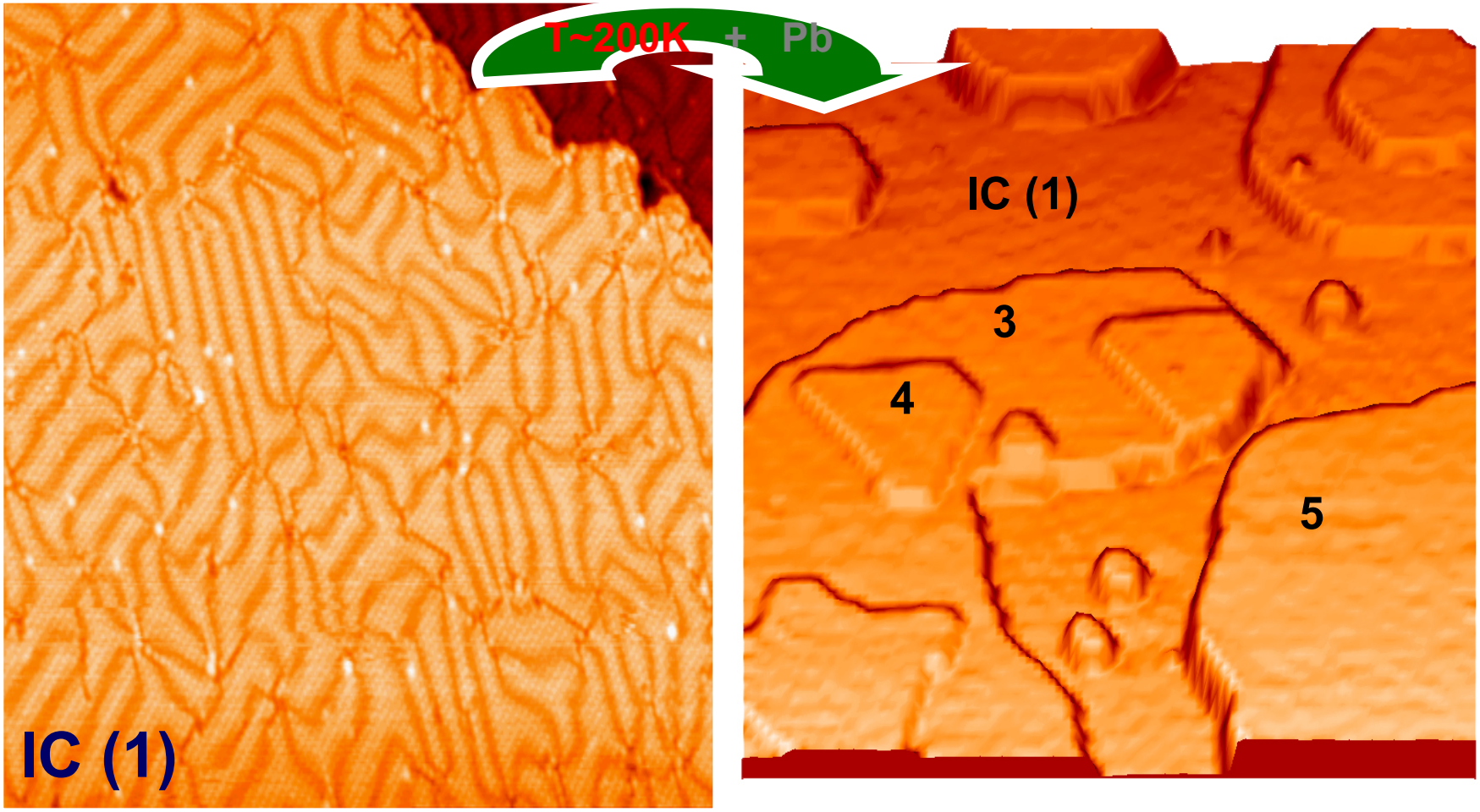

Spectra for Pb Films

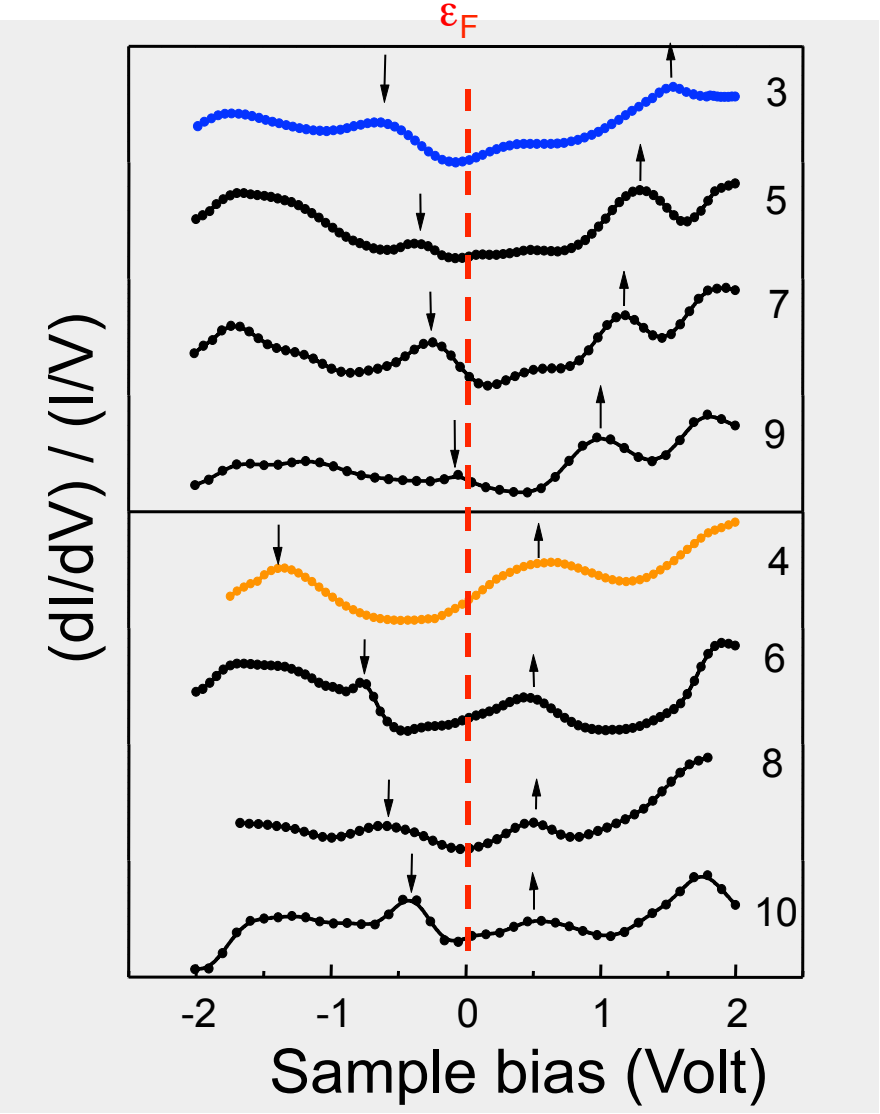

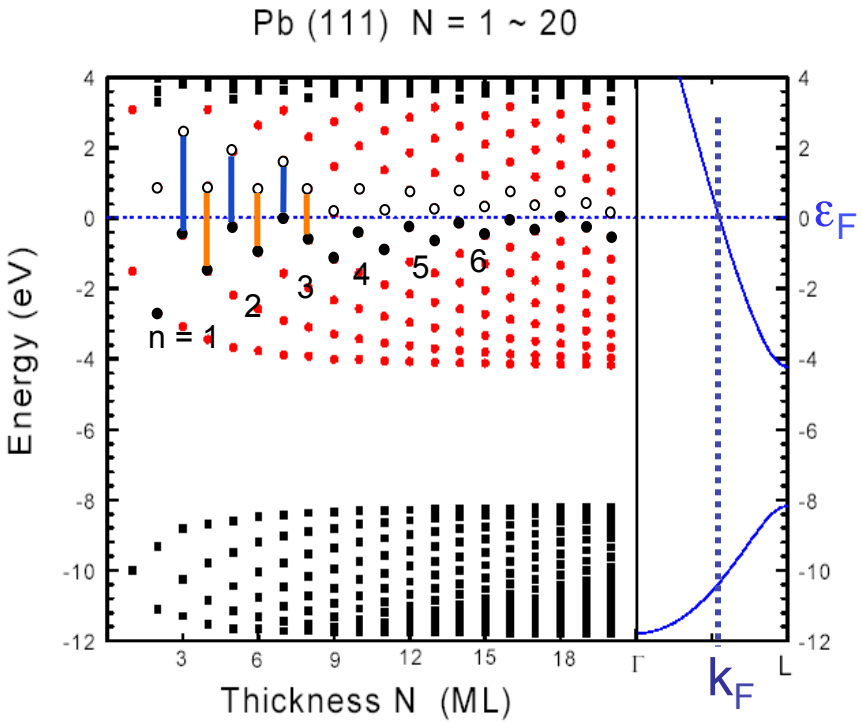

C.M. Wei and M.Y. Chou

$d_0 = 2.85$ Å $\lambda_F = 3.94$ Å

$2d_0 \approx 3(\lambda_F/2)$

Scanning Tunneling Spectroscopy (STS)

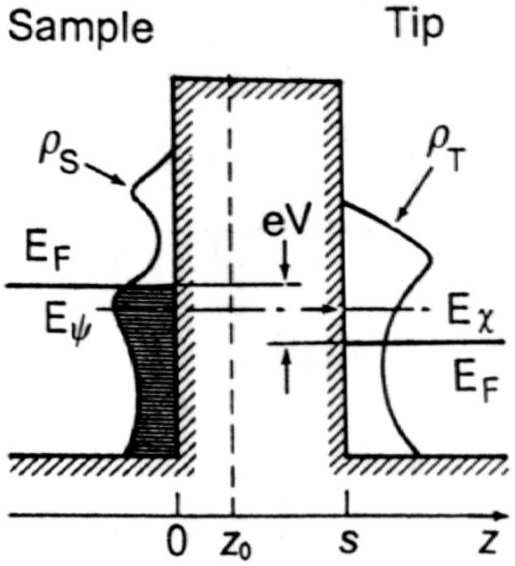

(feedback off)
I-V spectrum

(feedback on)
Z-V spectrum

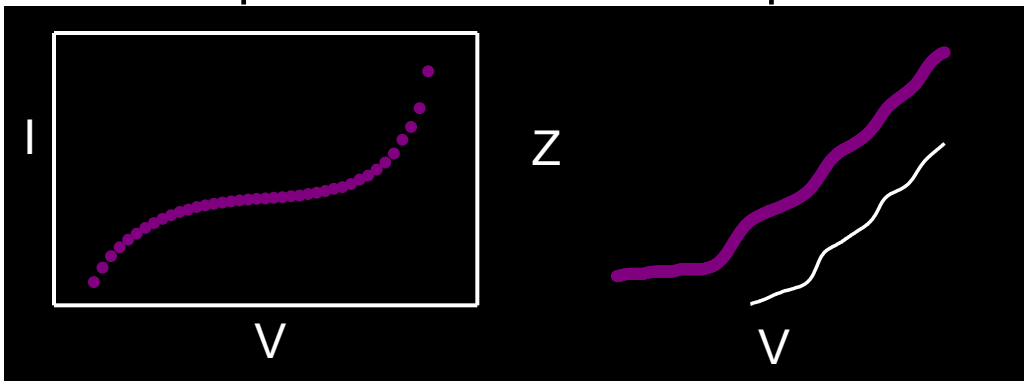

$$I \propto \int_0^{eV} \rho_s(E_F\text{-}eV+\varepsilon)\, \rho_T(E_F+\varepsilon) d\,\varepsilon$$

ρ_T is constant $\Rightarrow$ $dI/dV \propto \rho_s(E_F\text{-}eV)$

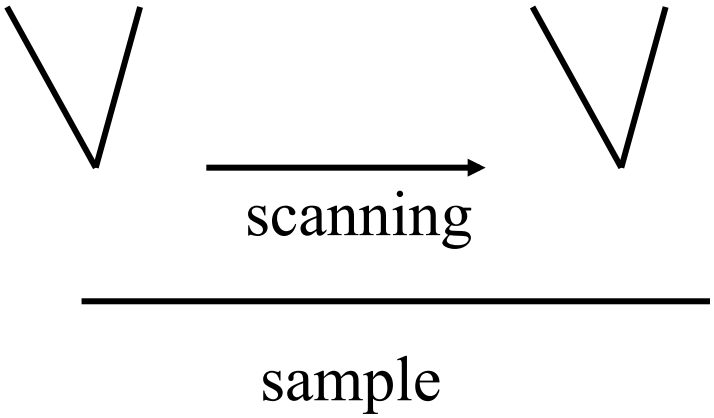

Gundlach Oscillation in STS

E_F of tip < E_{vac} of sample

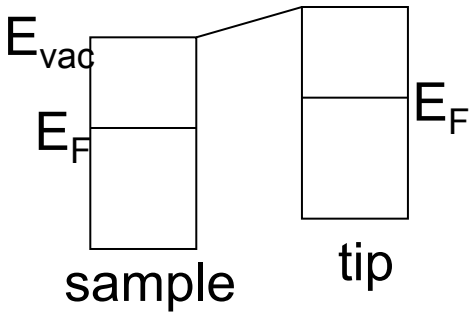

normal tunneling

E_F of tip > E_{vac} of sample

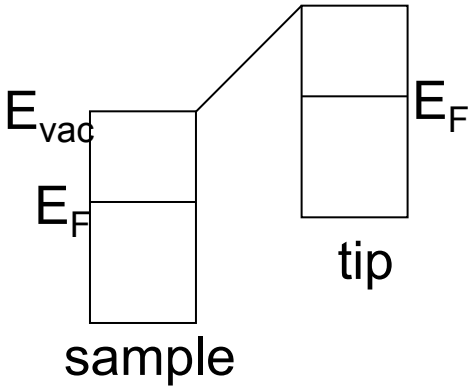

field emission

Standing-wave states
in tunneling gap

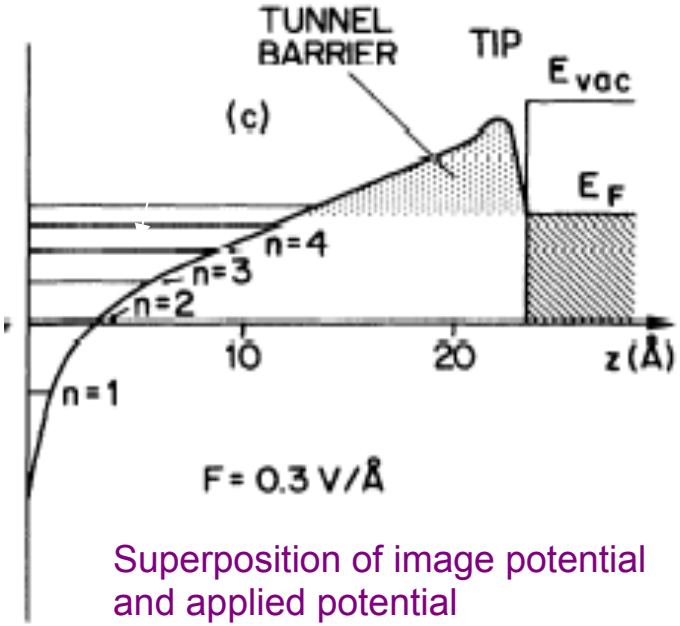

sample

Superposition of image potential
and applied potential

Transmission Resonance in Ag Films on Si(111)

Ag film on Si(111) at RT

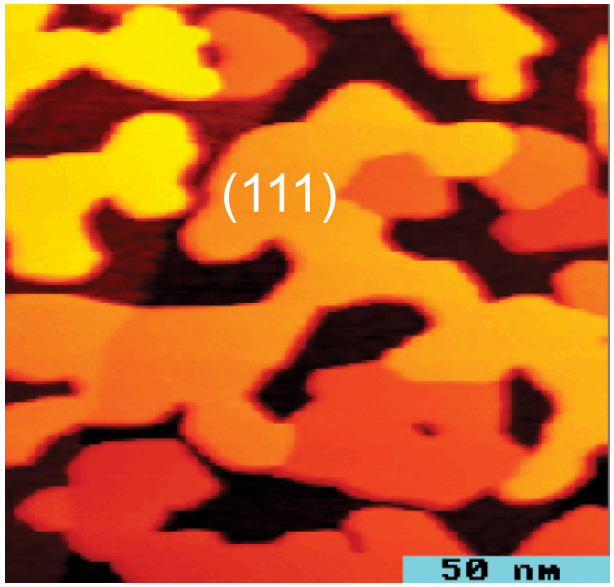

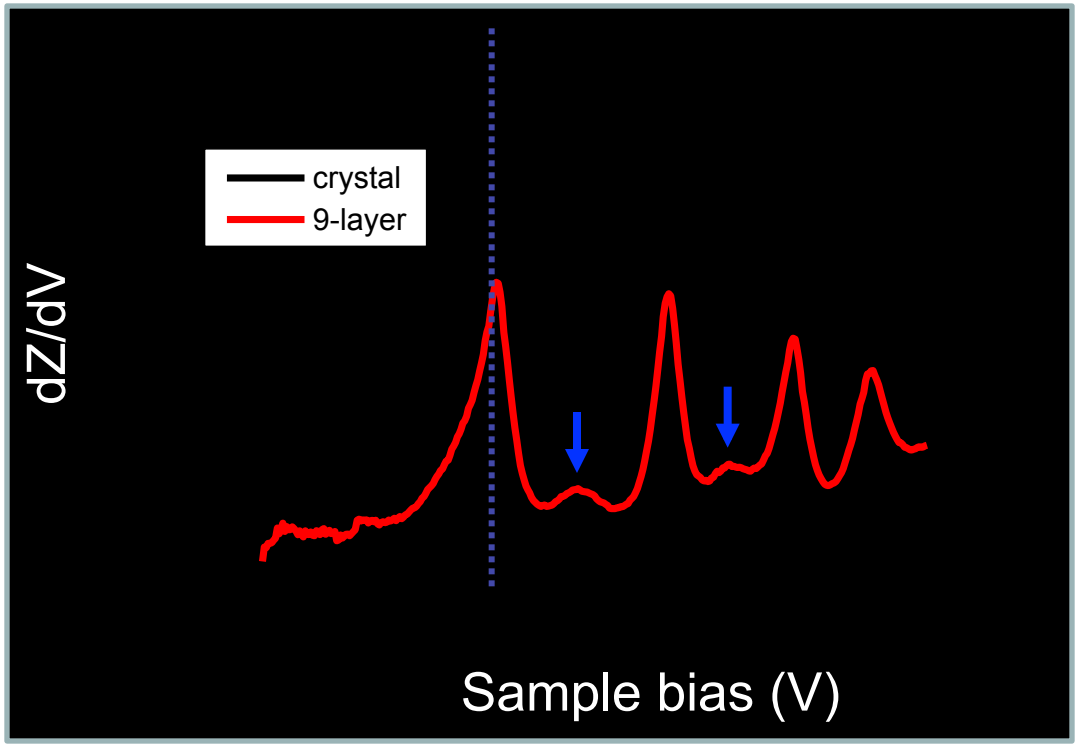

Work function of Ag/Si(111) = 4.41 eV

Quantum Size Effect above Vacuum Level

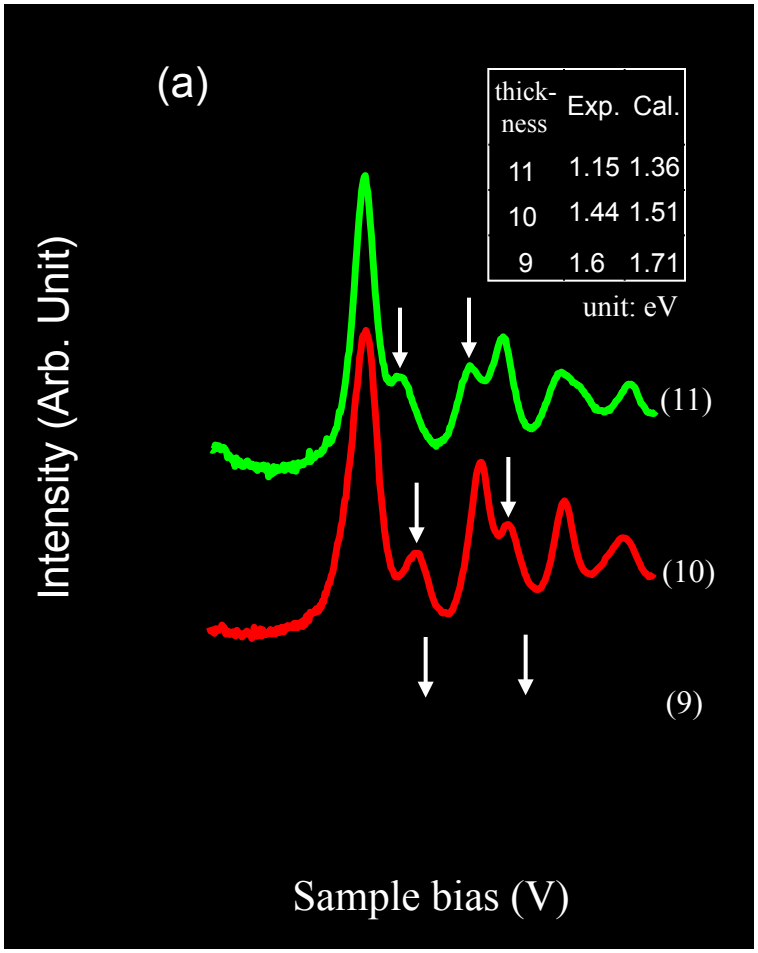

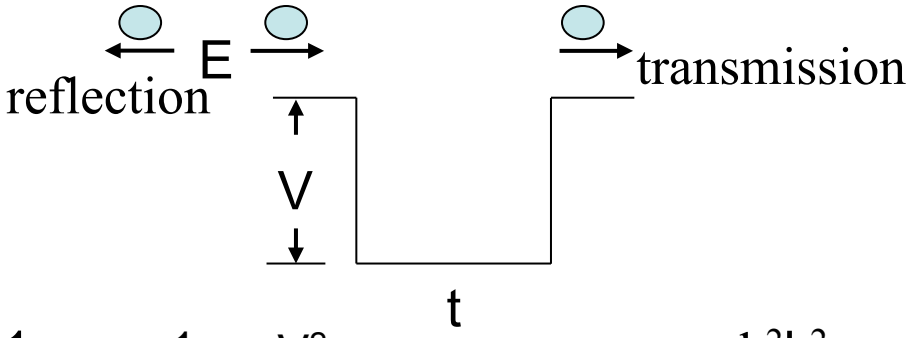

$$\frac{1}{T} = 1+\frac{1}{4}\frac{V^2}{E(E+V)}\sin^2(kt);\ R=1-T;\ \frac{\hbar^2k^2}{2m} = E+V$$

$kt=n\pi \rightarrow T=1$ transmission resonance

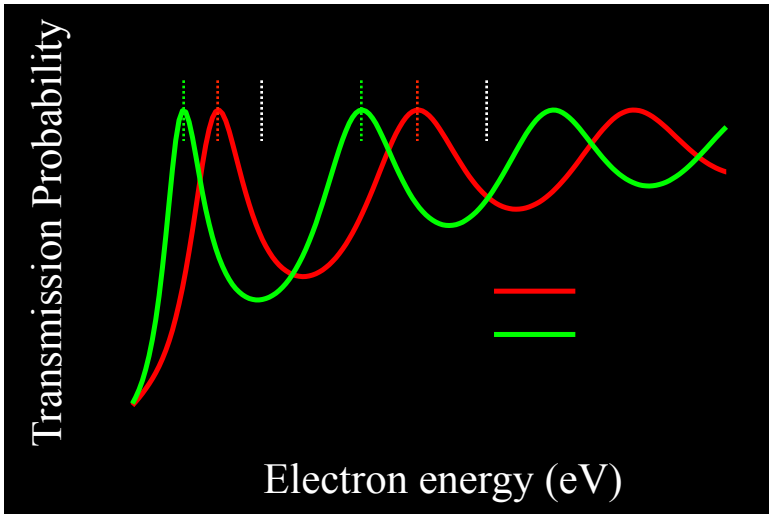

"Finger print" of film thickness

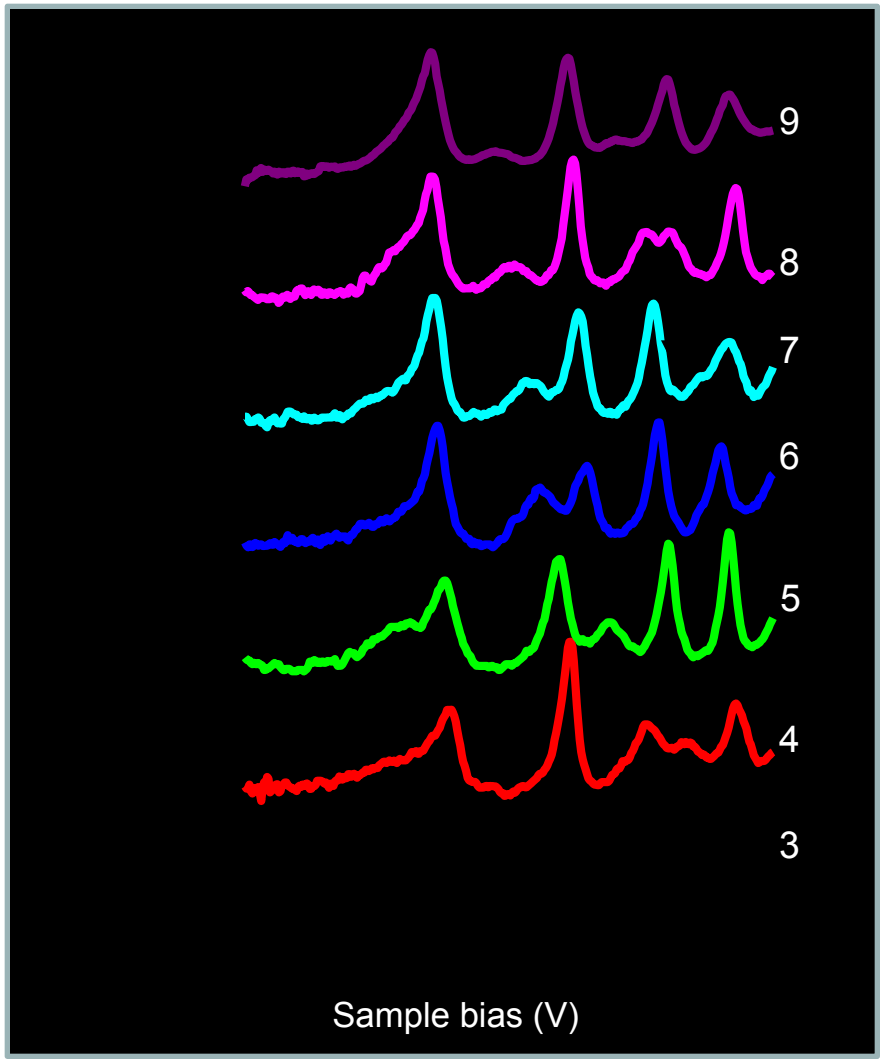

Low temperature deposition followed annealing to room temperature

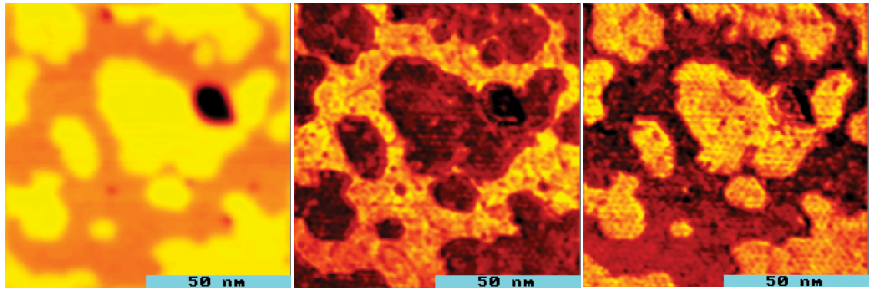

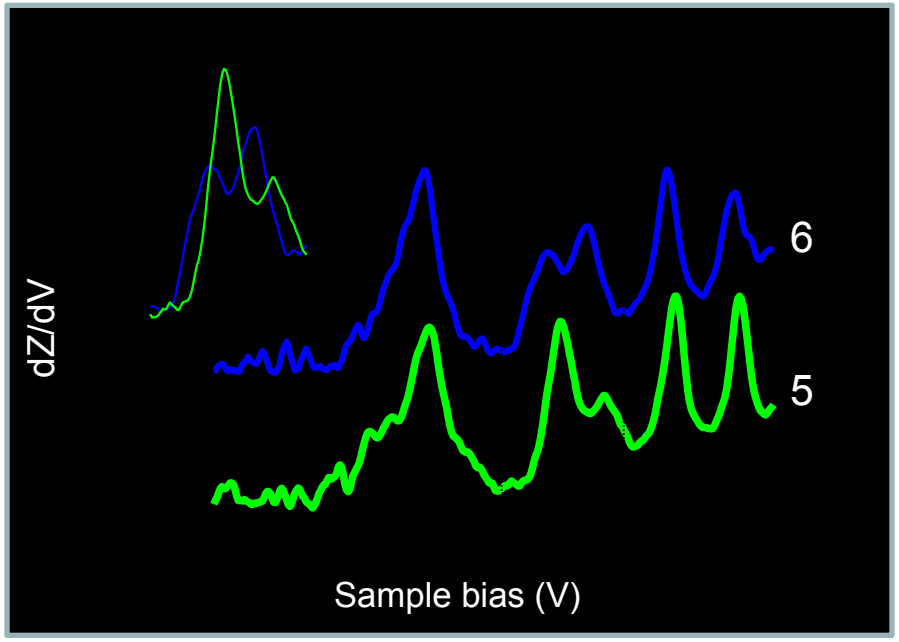

Summary

- *Quantum well states are measured with STS in the Pb films of varied thickness on the Si(111) surface.*

- *Quantum phenomenon of the transmission resonance can be observed with STS in Ag films on the Si(111) surface.*

- *Positions of the transmission resonance measured with STS can serve as finger prints for the Ag films of varied thickness.*

Work function measurements for thin films

work function measurement for thin film using photo-emission spectroscopy

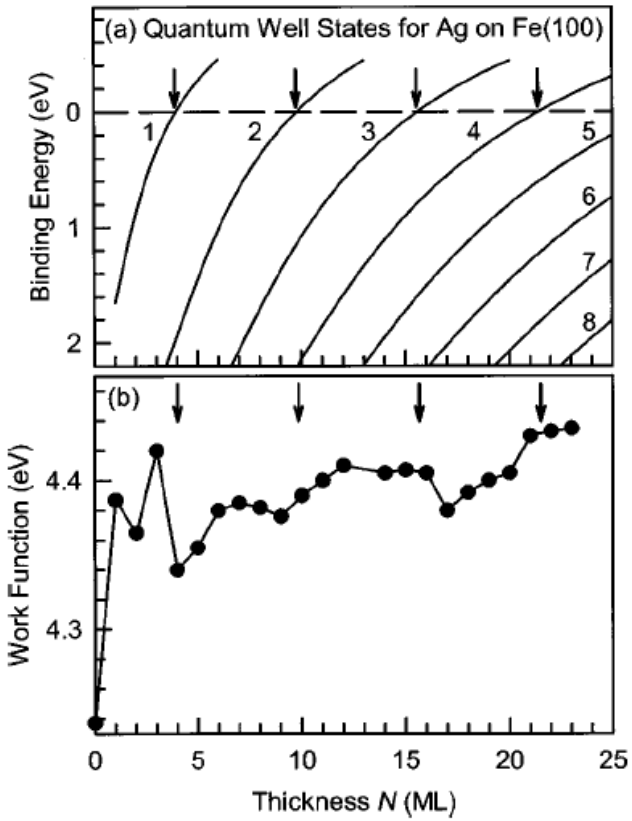

J. J. Paggel et al. 66, Phys. Rev. B (2002) 233403.

Broad beam technique

require layer by layer growth

Average work function of various thickness

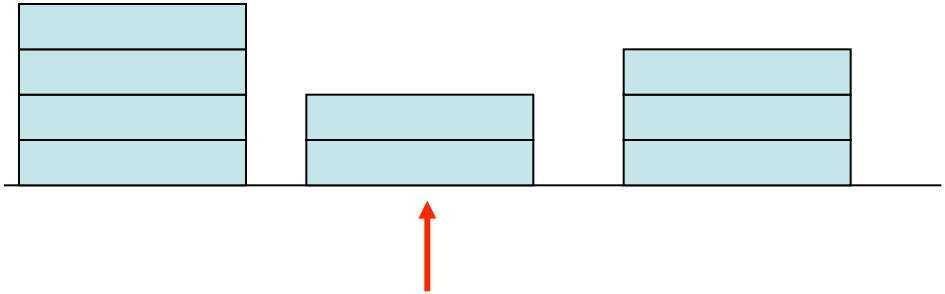

Local probe technique, e.g. STM

Constant Energy Shift

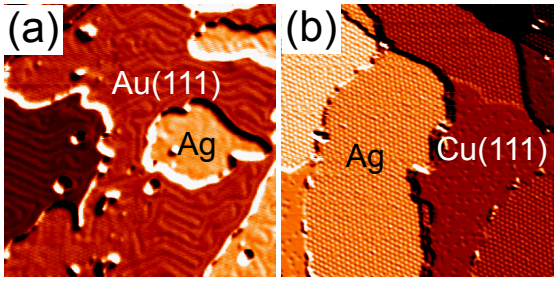

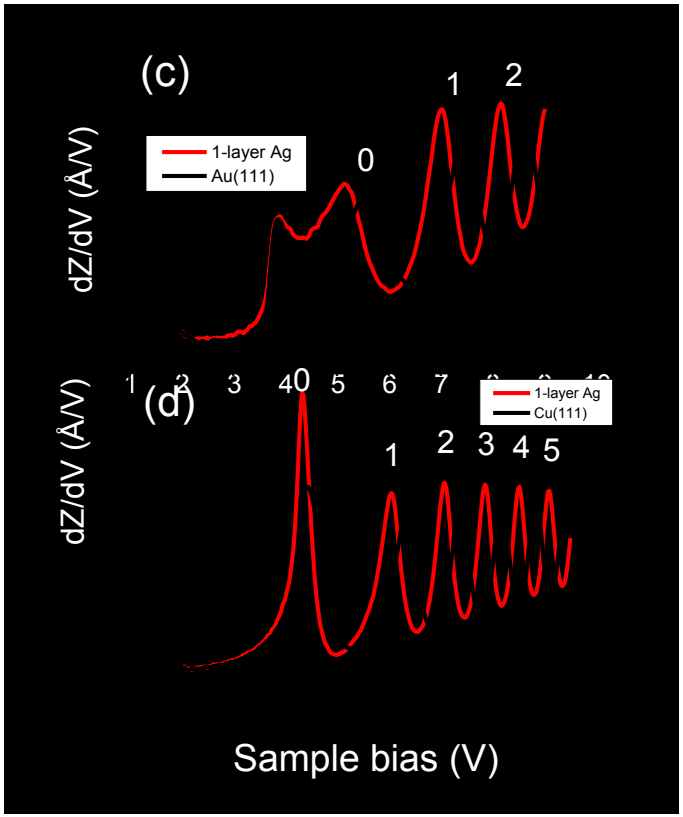

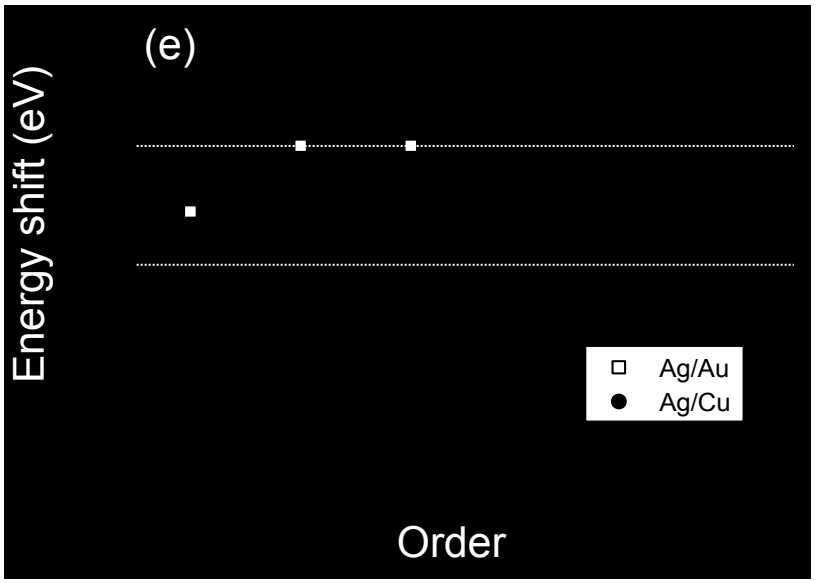

-0.47 eV

-0.3 eV

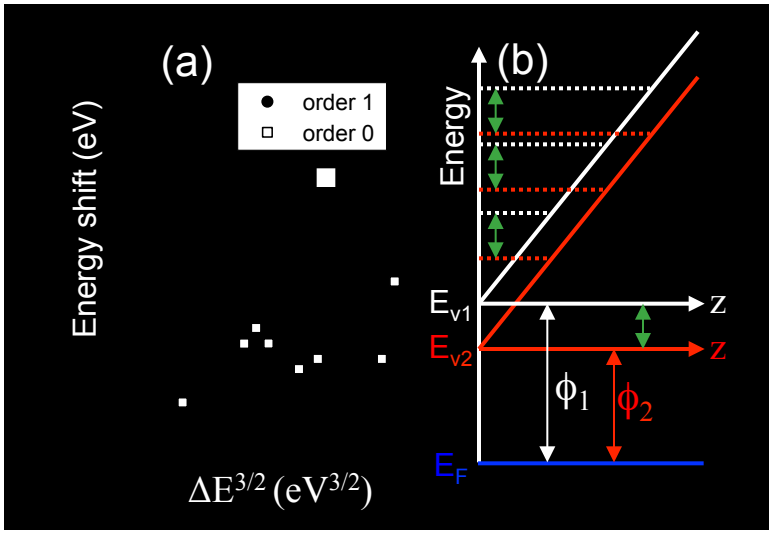

Lin et al., Phys. Rev. Lett. 99, 216103 (2007)

Comparison with PES measurement

Photoemission (-0.33 eV)

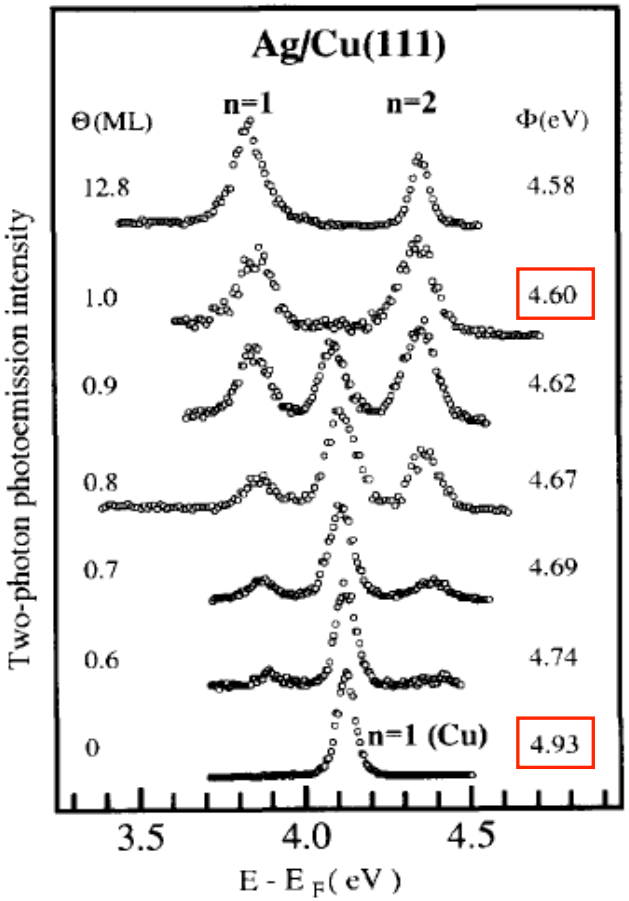

Wallauer et al., Surf. Sci 331, 731 (1995)

Gundlach oscillation (-0.3 eV)

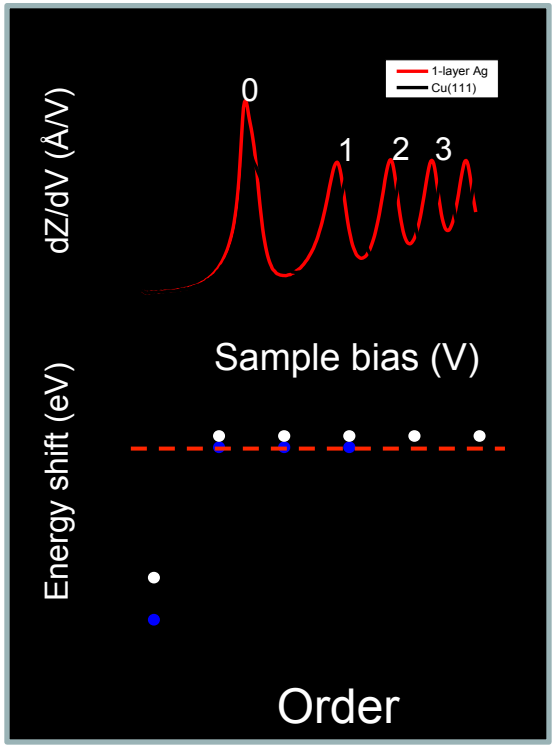

Bulk Materials	Φ(eV)
Au(111)	5.31
Ag(111)	4.74
Cu(111)	4.98

Summary

- *A general phenomenon of the constant energy shift is observed in high order Gundlach oscillation.*

- *The work function of a thin metal film can be measured with the constant energy shift.*

- *The precision of the measurement can be better than 0.02 eV, comparable to the photoemission results.*

Vibrational Spectroscopy

1. Photons in, photons out – IR, Raman
2. Electrons in, electrons out – EELS

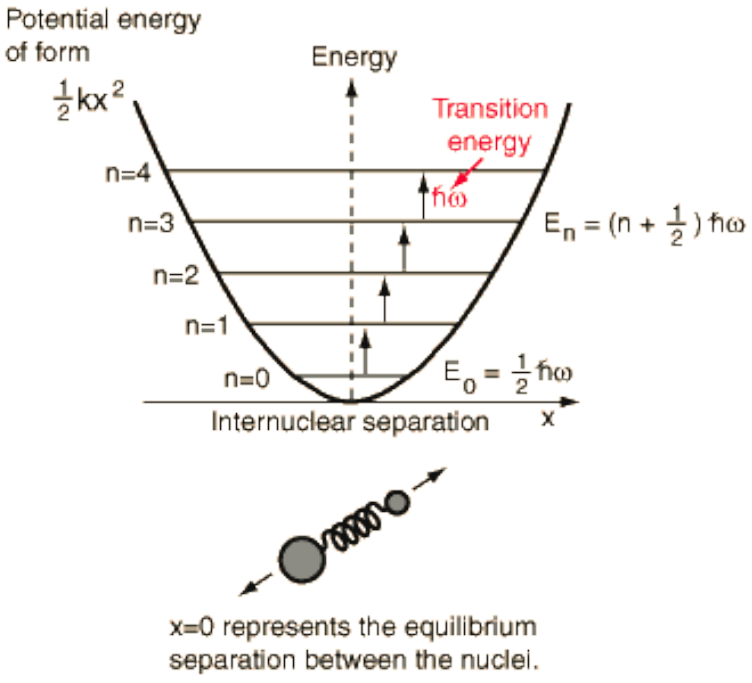

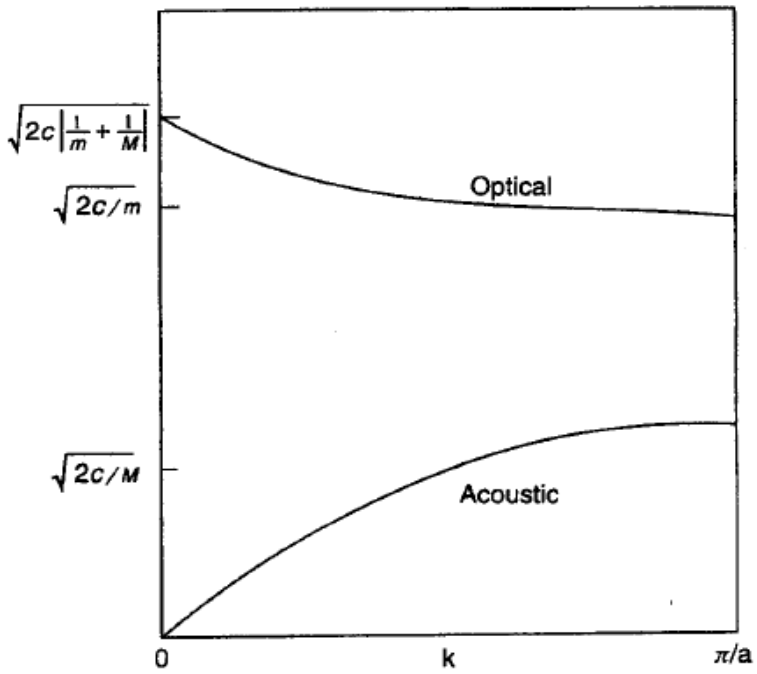

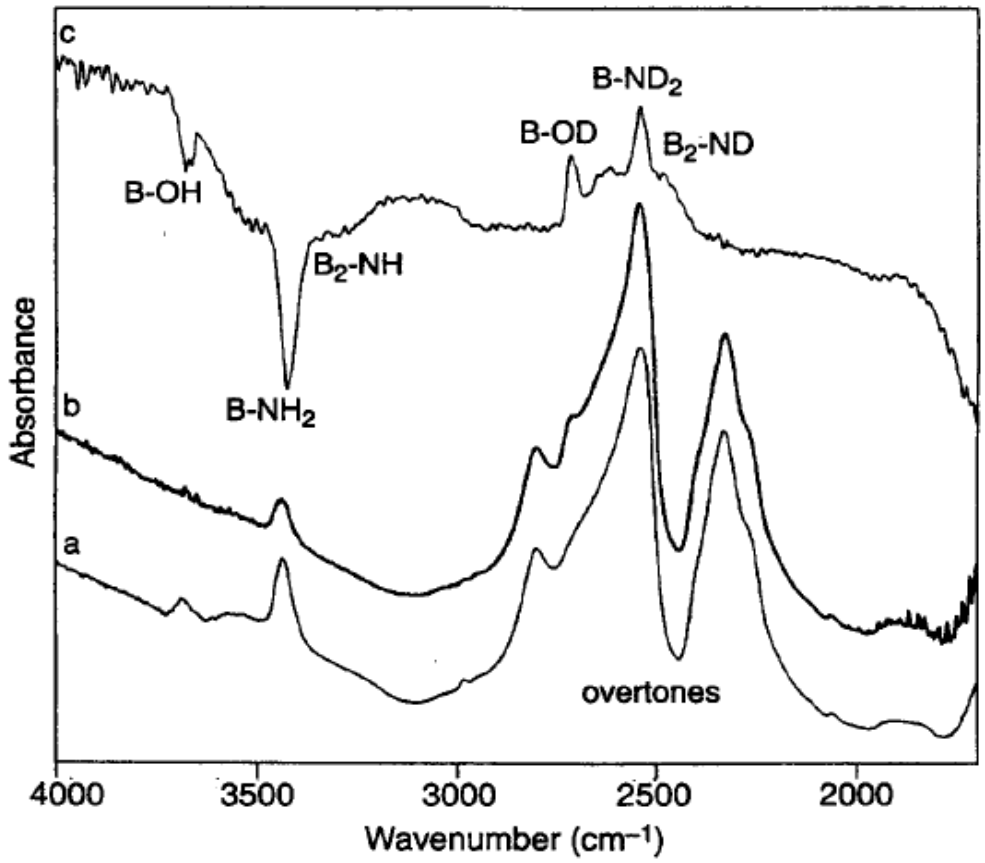

Figure 8.5. FTIR spectra of boron nitride nanopowder surfaces after activation at 875 K (tracing a), after subsequent deuteration (tracing b), and (c) difference spectrum of *a* subtracted from *b* (tracing c). [From M.-I. Baraton and L. Merhari, P. Quintard, V. Lorezenvilli, *Langmuir*, **9**, 1486 (1993).]

Optical properties of nanoparticles (in the infrared range)

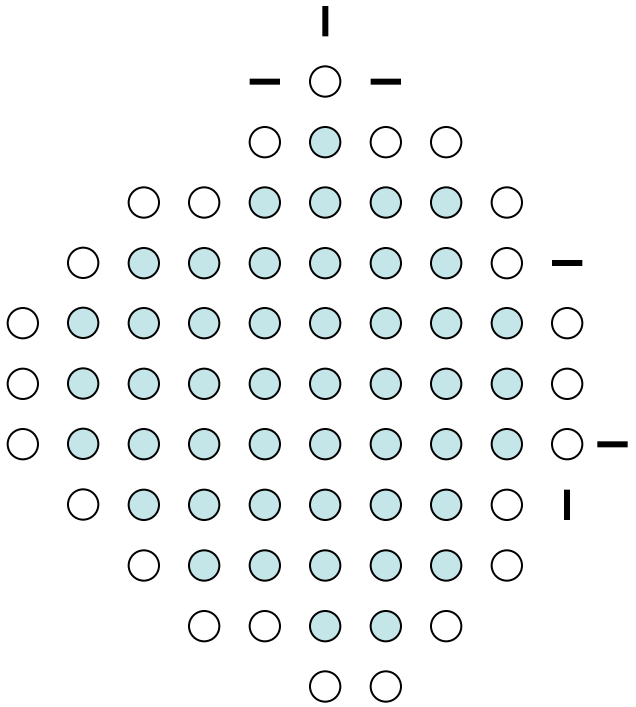

(1) Broad-band absorption:
Due mainly to the increased normal modes at the surface.

(2) Blue shift:
Due mainly to the bond shortening resulted from surface tension.

The Theory of Raman Spectroscopy

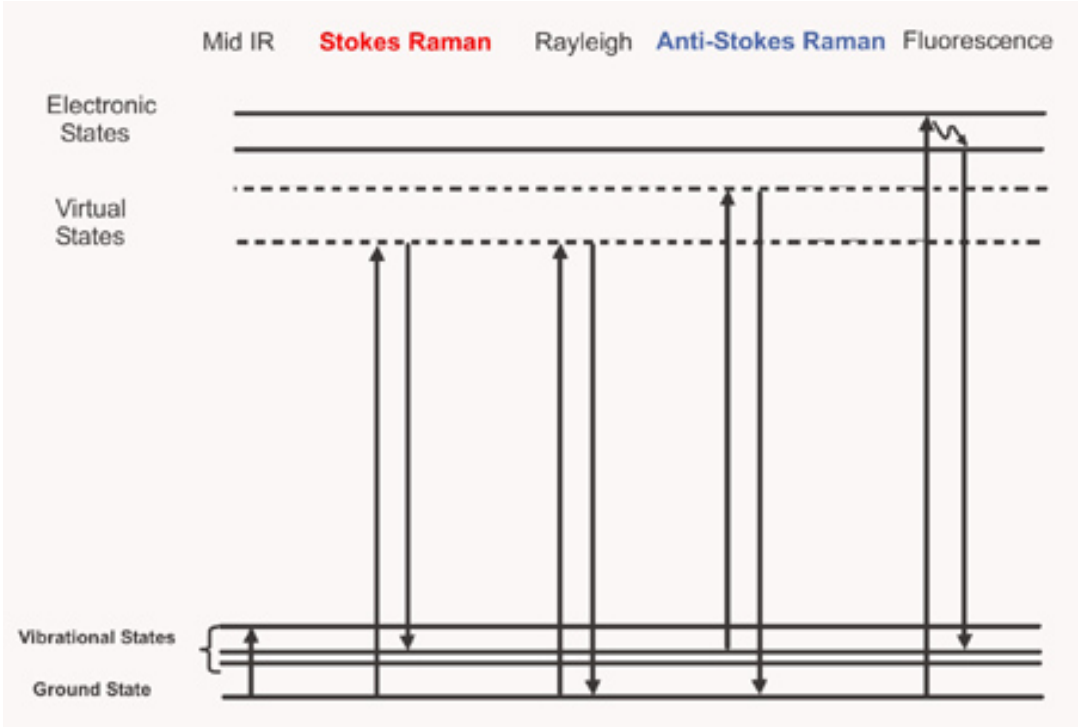

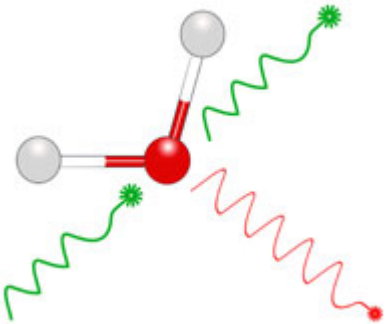

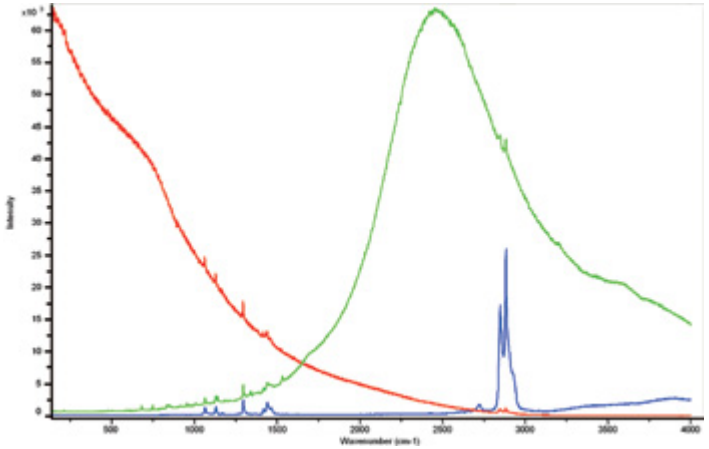

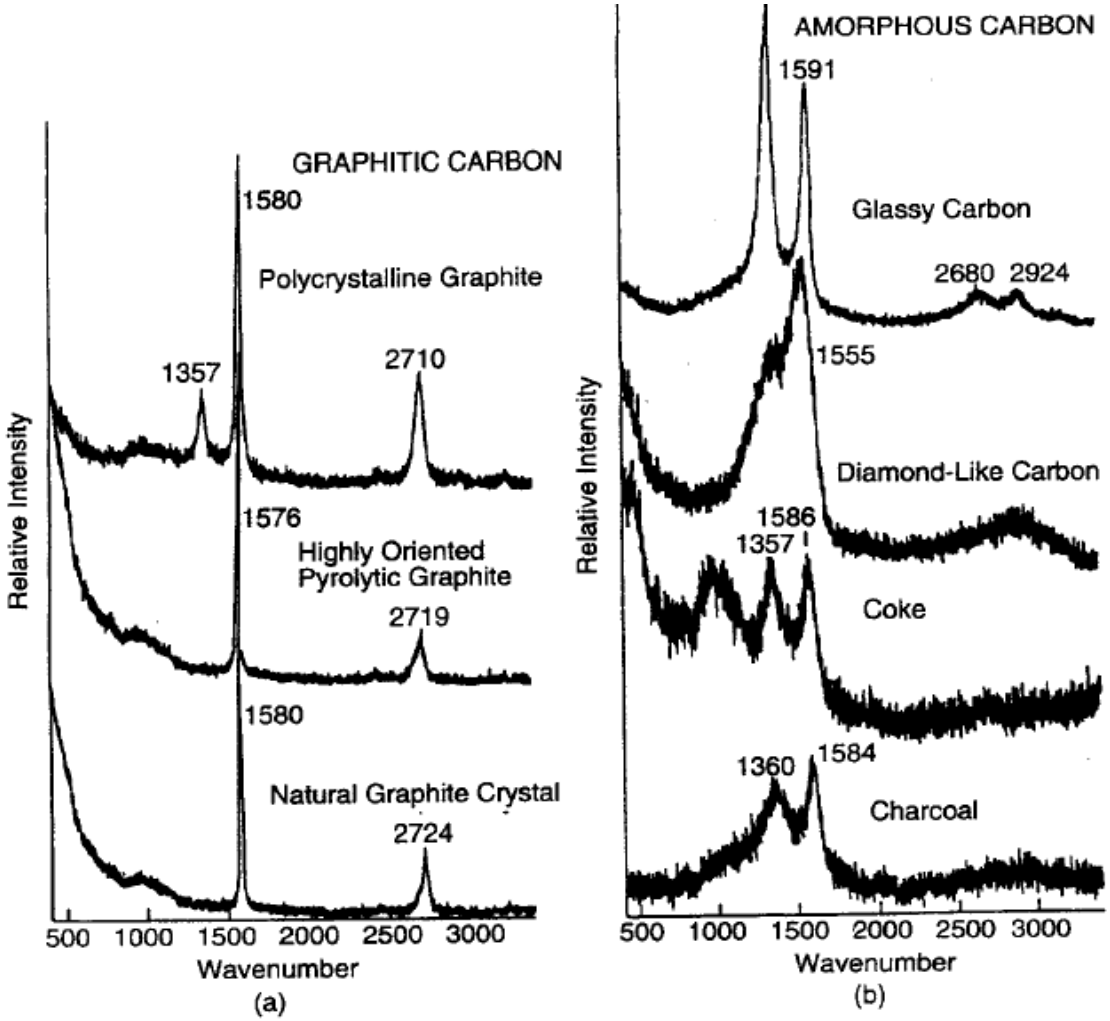

Figure 8.19. Raman spectra of (a) crystalline graphites and (b) noncrystalline, mainly graphitic, carbons. The *D* band appears near 1355 cm^{-1} and the *G* band, near 1580 cm^{-1}. [From D. S. Knight and W. B. White, *J. Mater, Sci.* **4**, 385 (1989).]

Inelastic Tunneling

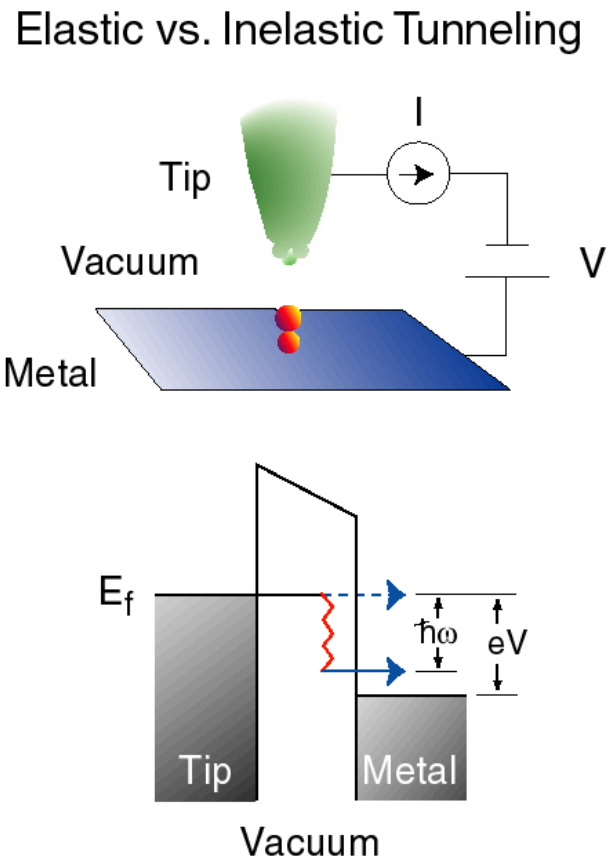

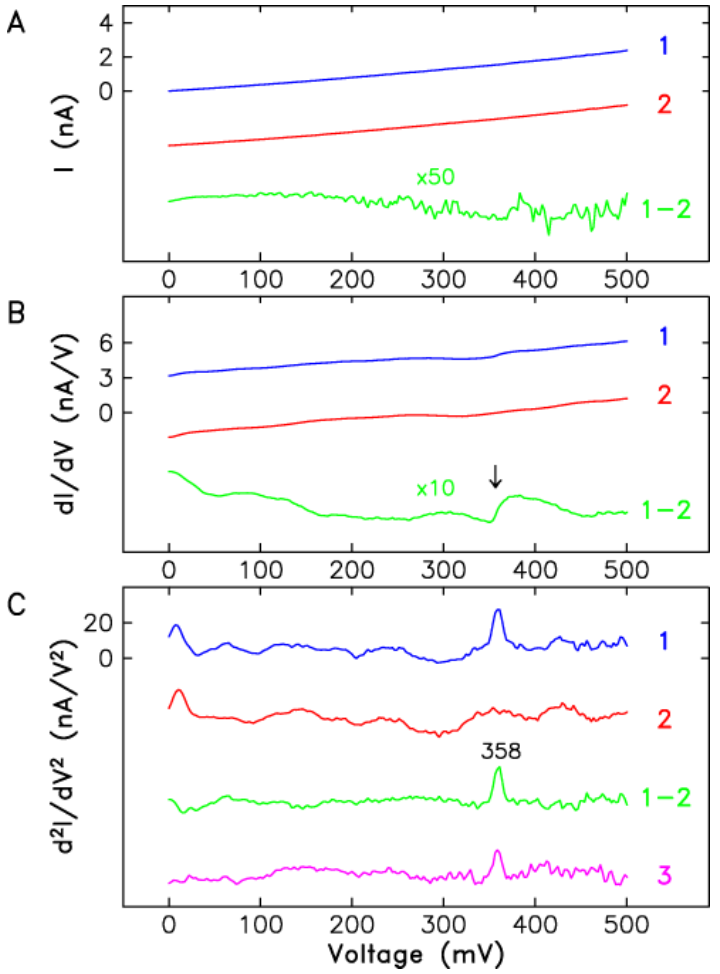

Single Molecule Vibrational Spectroscopy and Microscopy

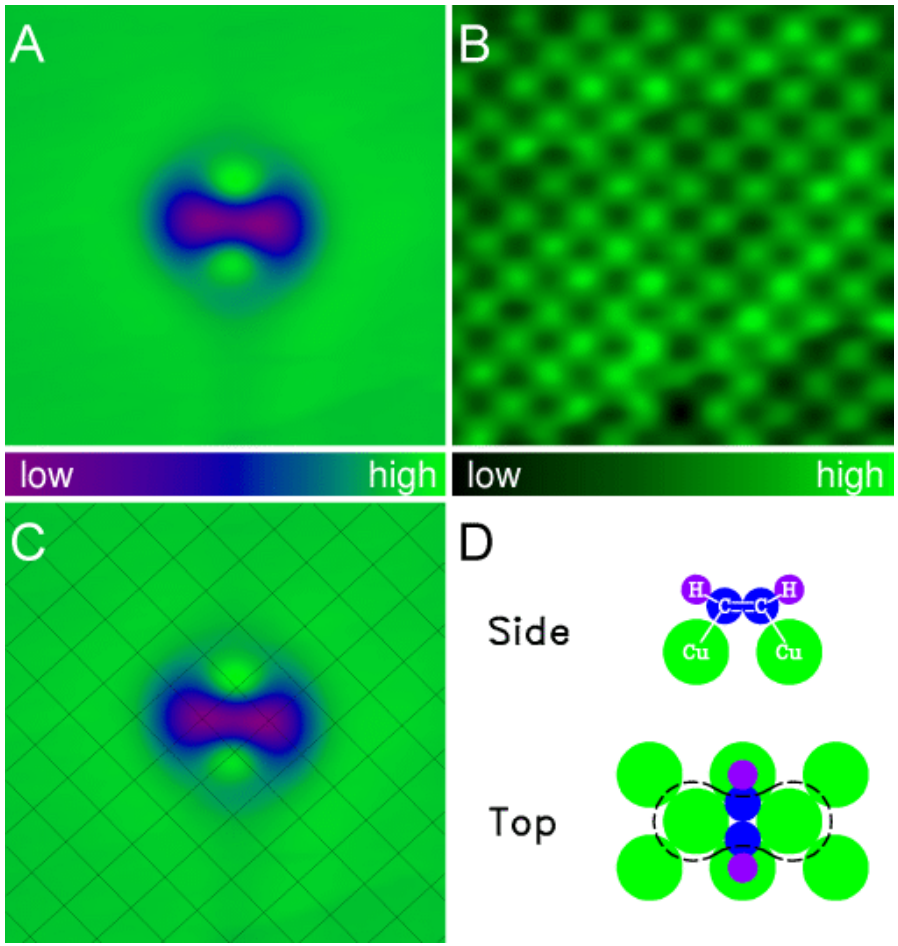

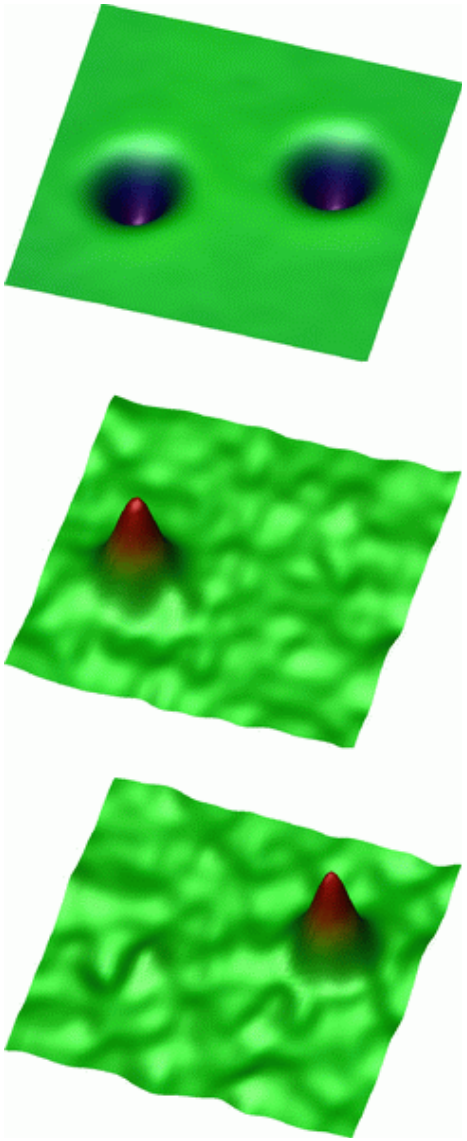

B.C. Stipe, M.A. Rezaei, and W. Ho,
Science **280**, 1732-1735 (1998).

Atomic Scale Coupling of Photons to Single-Molecule Junctions

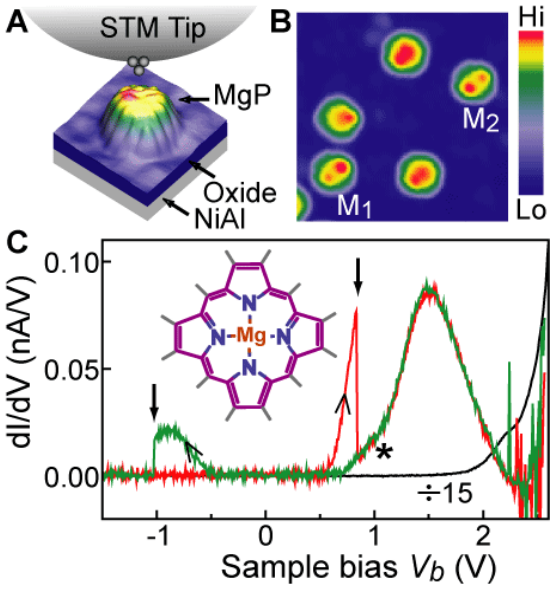

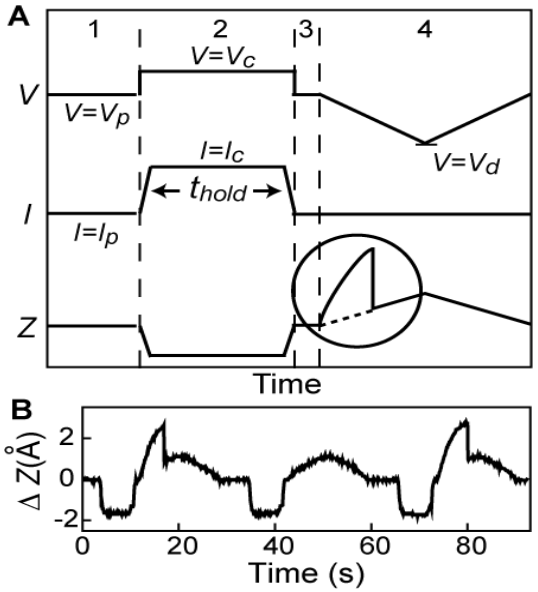

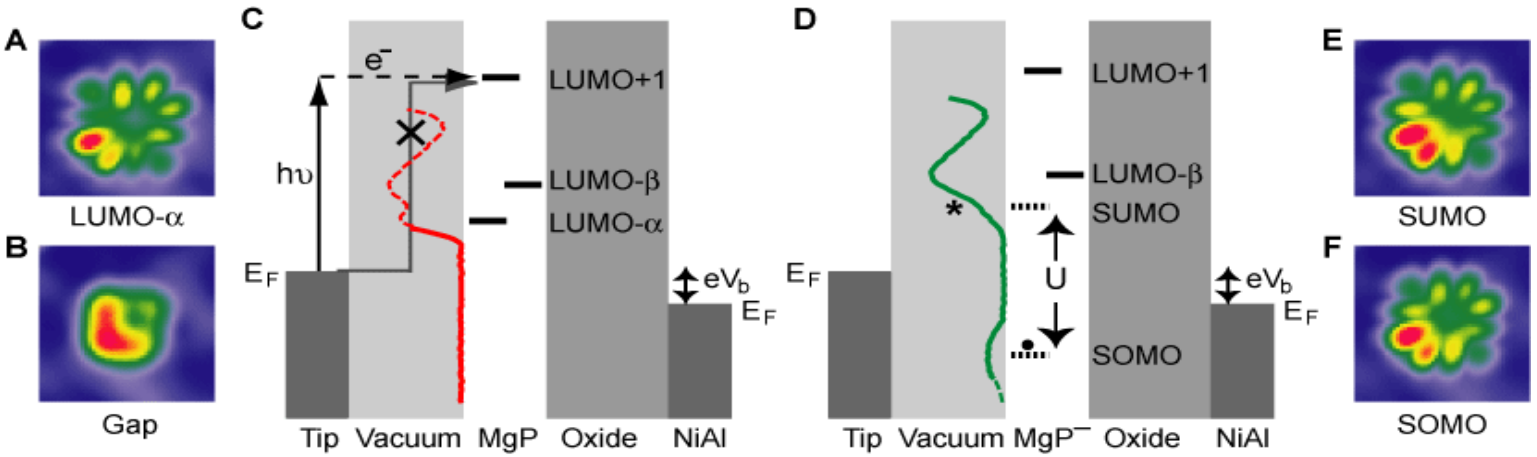

S.W. Wu and N. Ogawa and W. Ho, Science **312**, 1362-1365 (2006)

Quantum corral

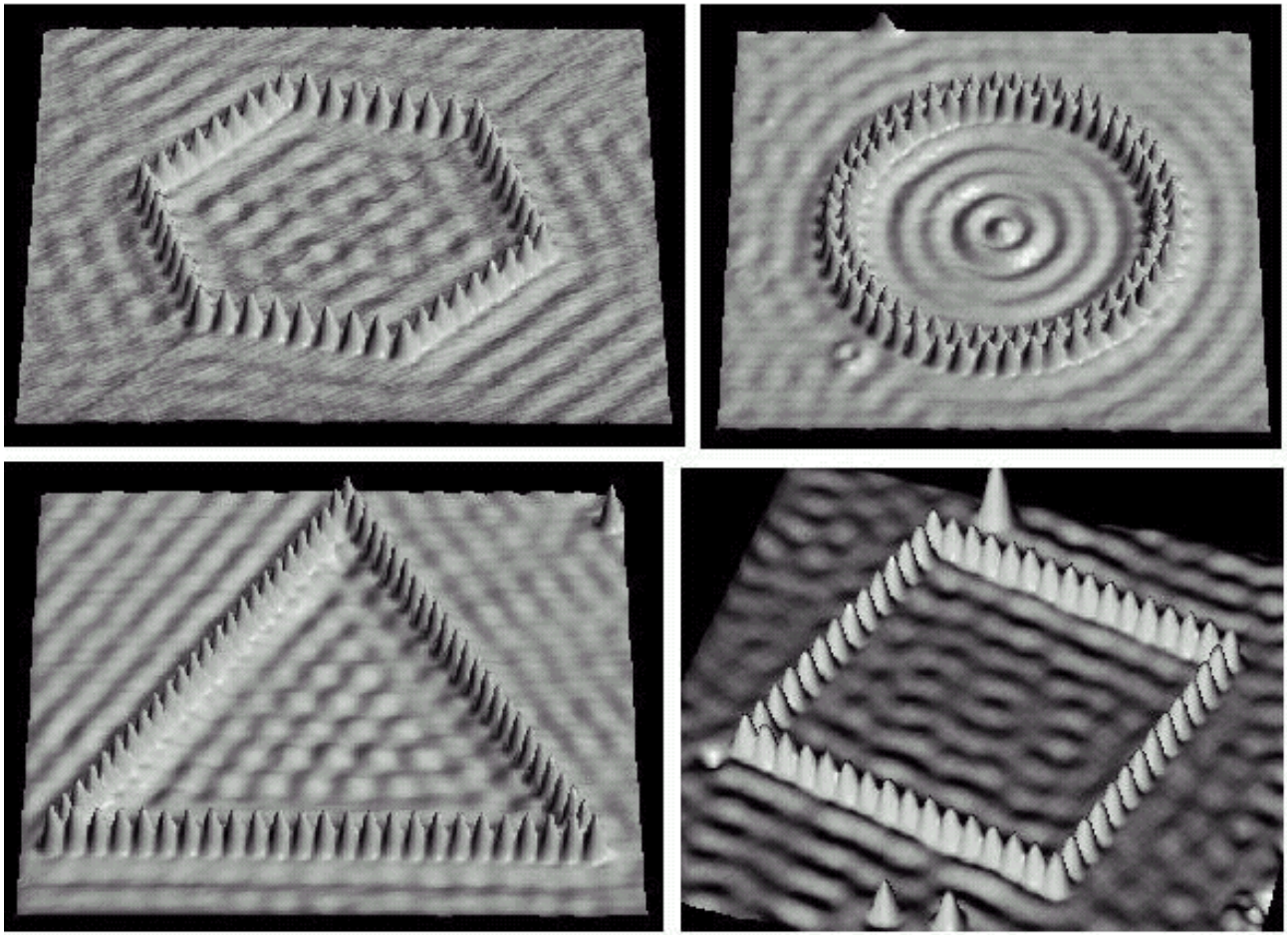

D.M. Eigler, IBM, Amaden

Artificial atom

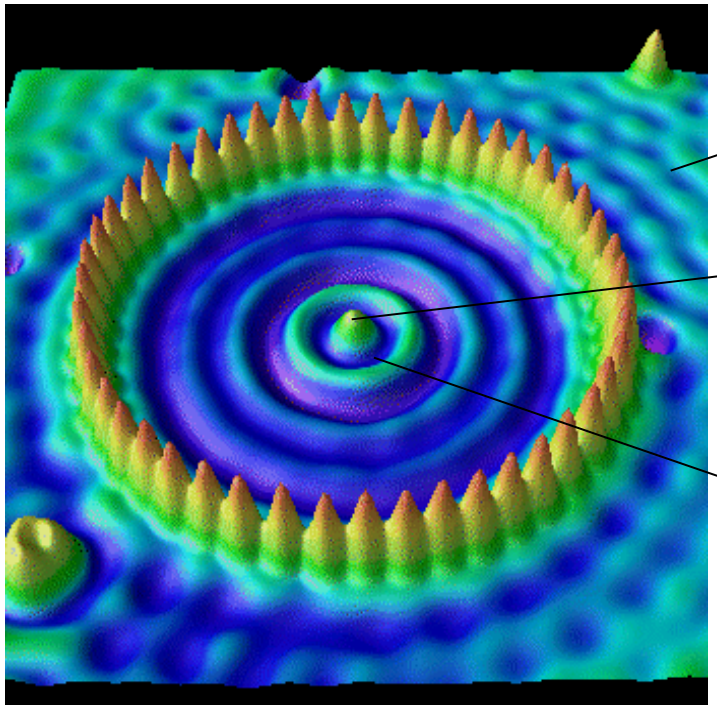

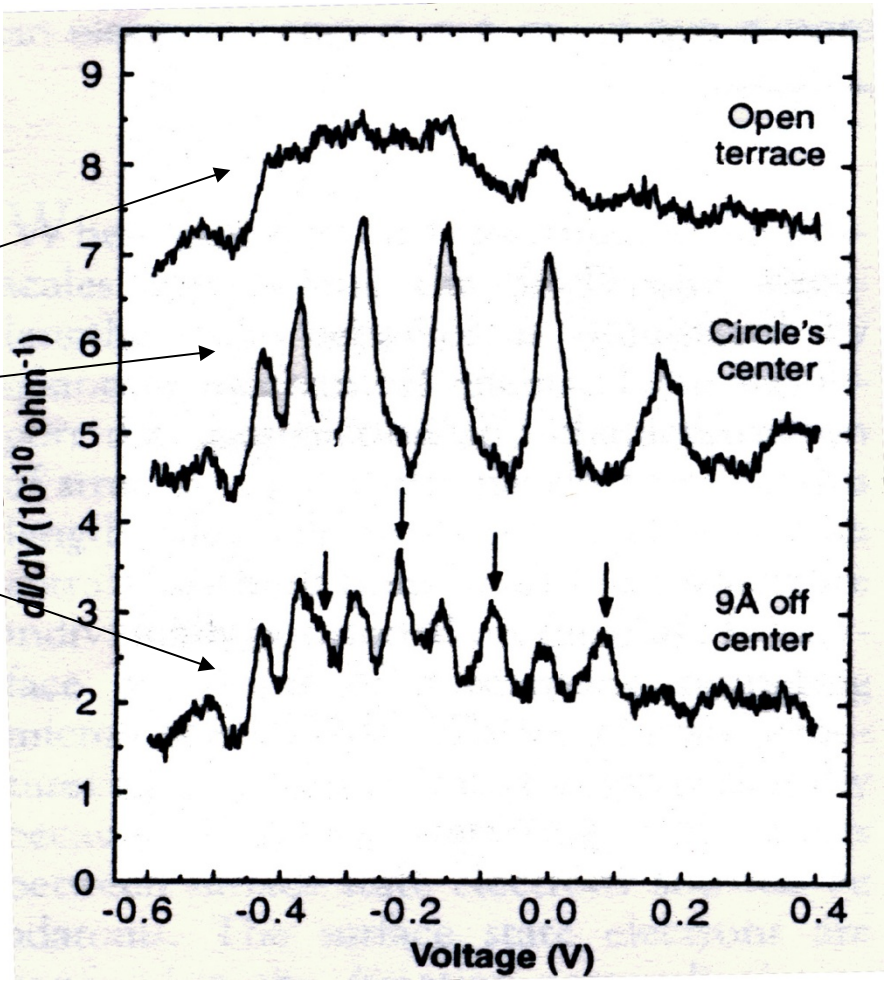

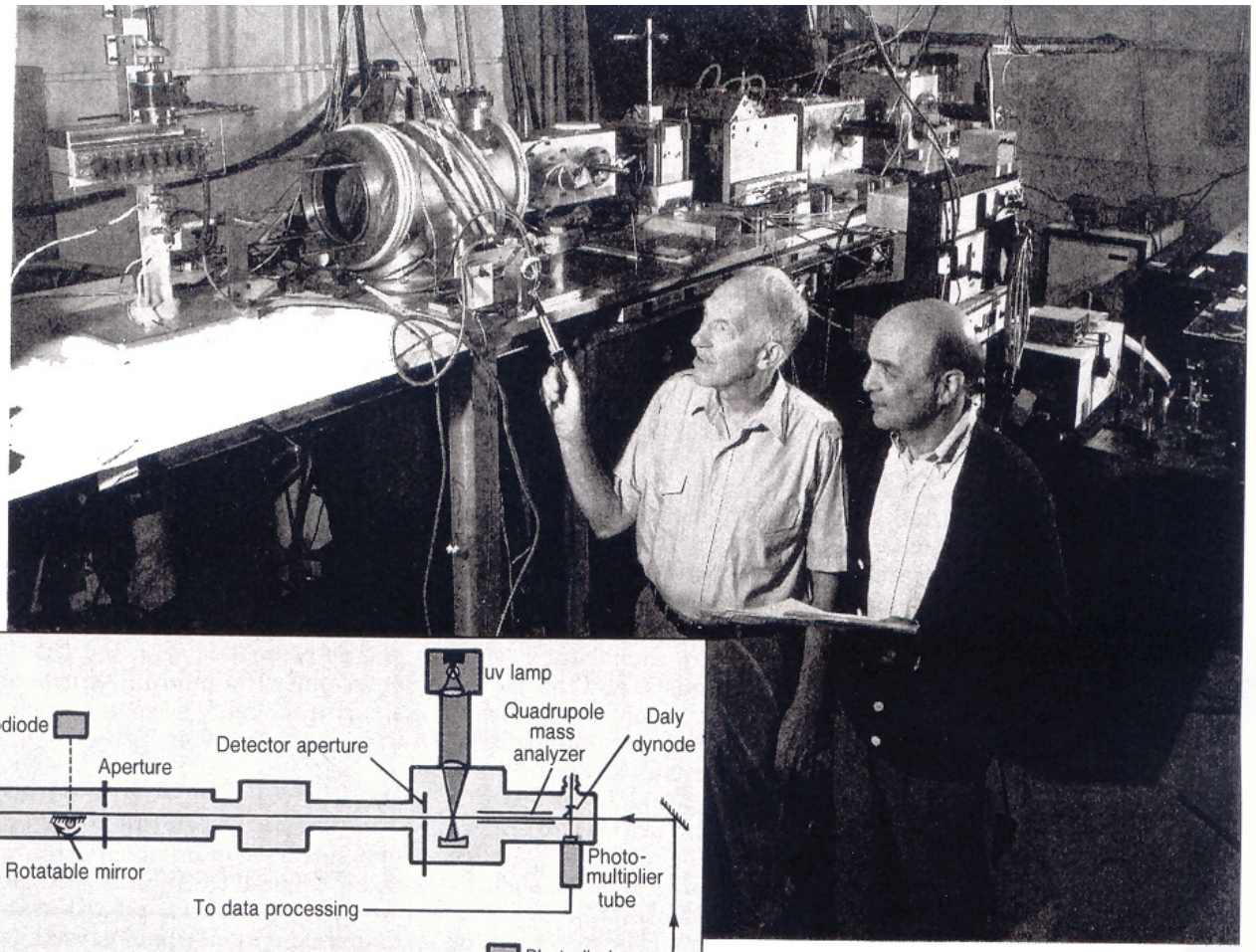

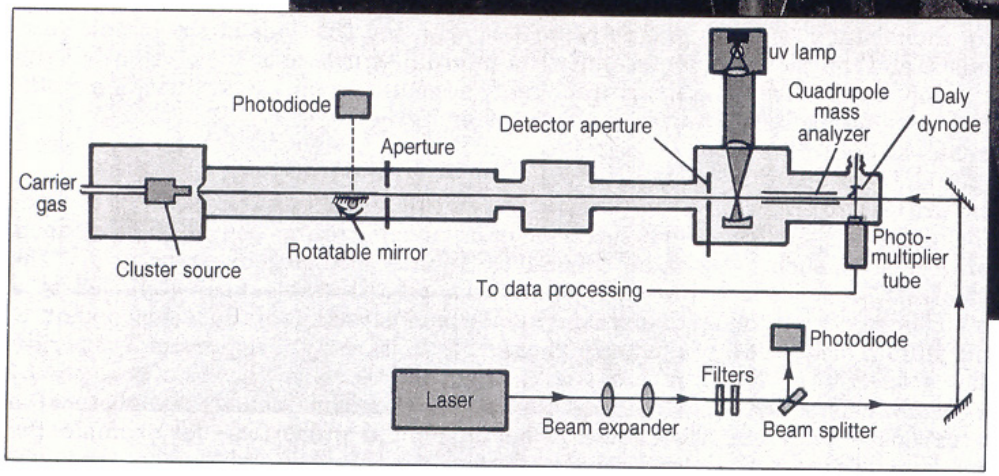
uv lamp
Photodiode
Quadrupole mass analyzer
Daly dynode
Detector aperture
Aperture
Carrier gas
Photo-multiplier tube
Rotatable mirror
Cluster source
To data processing
Photodiode
Filters
Laser
Beam expander
Beam splitter

Mass Analyzer

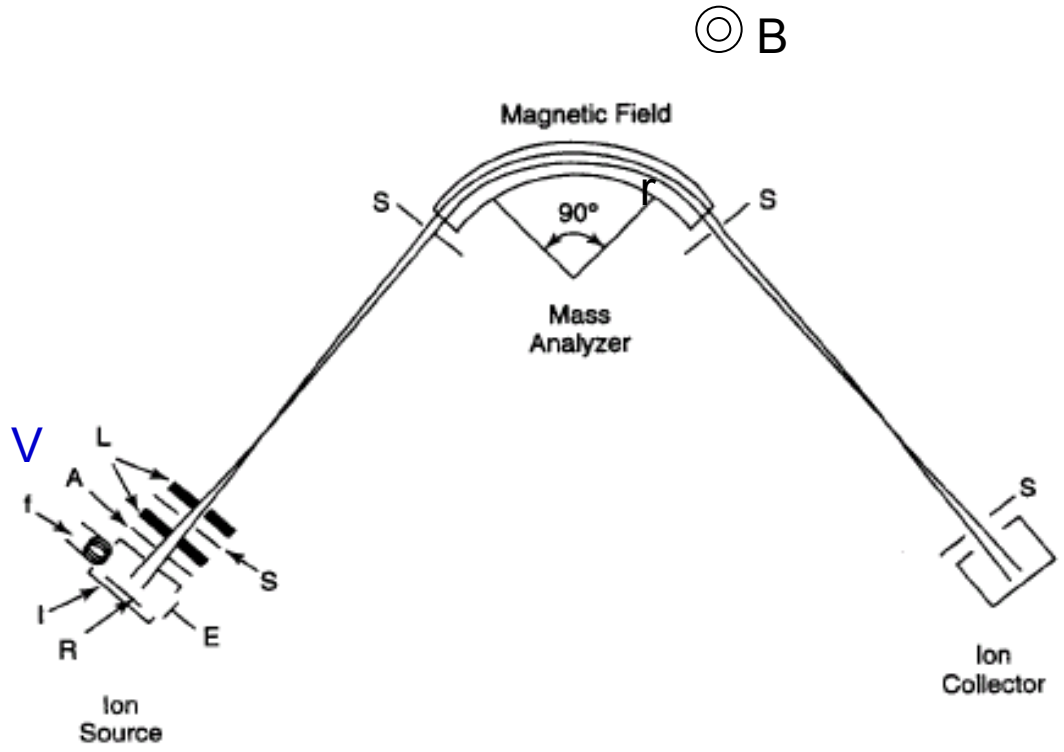

Figure 3.8. Sketch of a mass spectrometer utilizing a 90° magnetic field mass analyzer, showing details of the ion source: A—accelerator or extractor plate, E—electron trap, f—filament, I—ionization chamber, L—focusing lenses, R—repeller, S—slits. The magnetic field of the mass analyzer is perpendicular to the plane of the page.

$qV = \frac{1}{2} mv^2$

$F = qvB = mv^2/r$

$m/q = \frac{1}{2} B^2r^2/V$

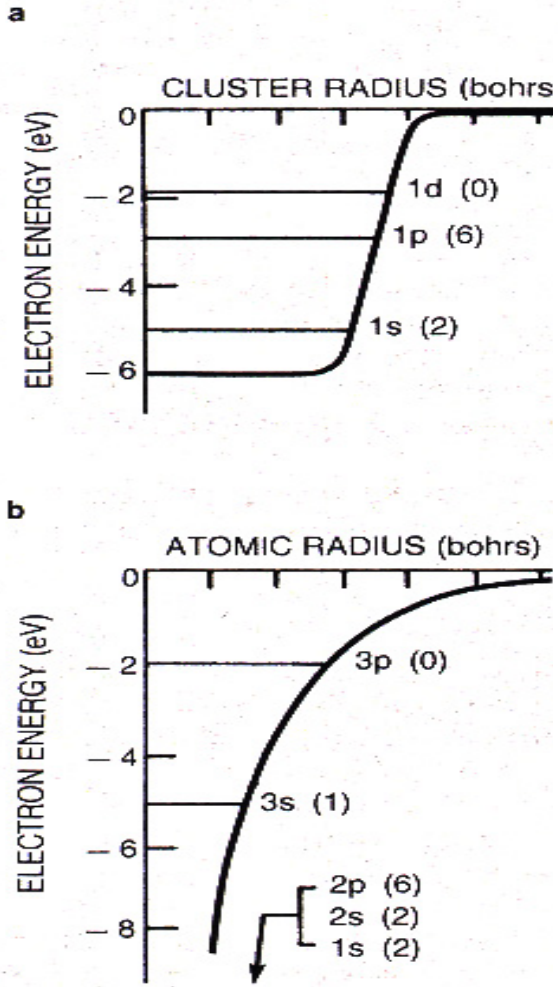

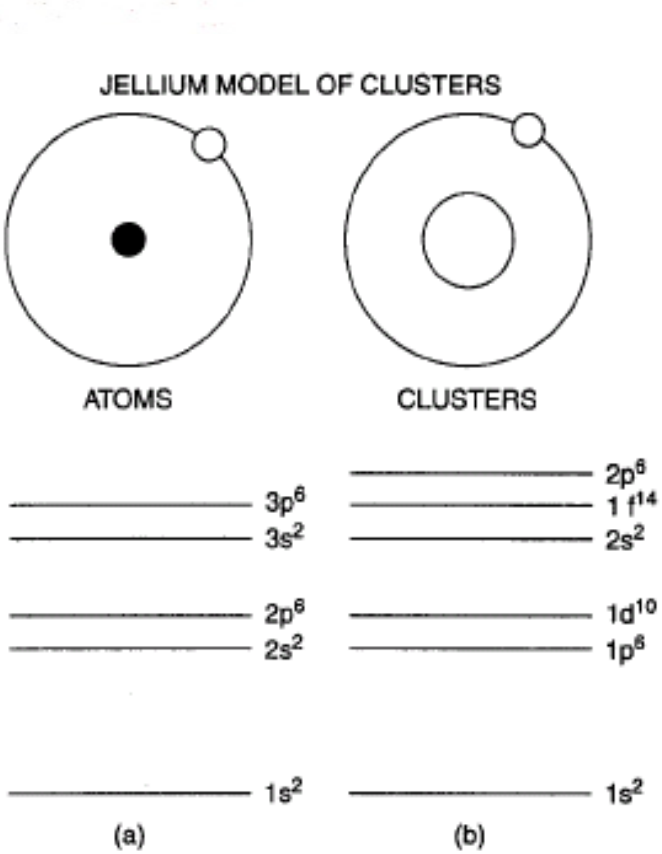

Figure 4.5. A comparison of the energy levels of the hydrogen atom and those of the jellium model of a cluster. The electronic magic numbers of the atoms are 2, 10, 18, and 36 for He, Ne, Ar, and Kr, respectively (the Kr energy levels are not shown on the figure) and 2, 18, and 40 for the clusters. [Adapted from B. K. Rao et al., *J. Cluster Sci.* **10**, 477 (1999).]

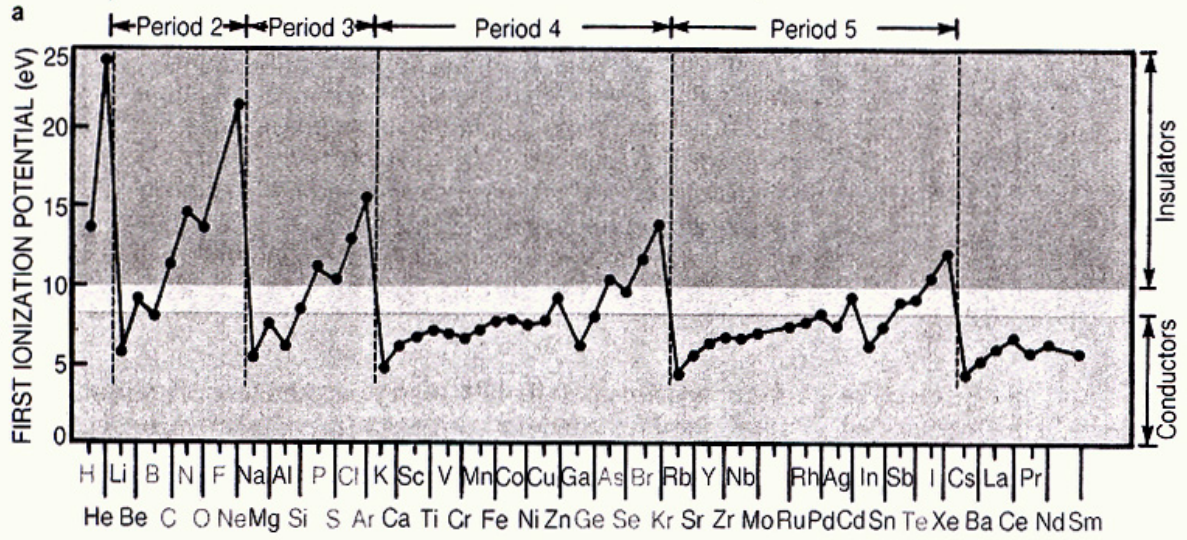

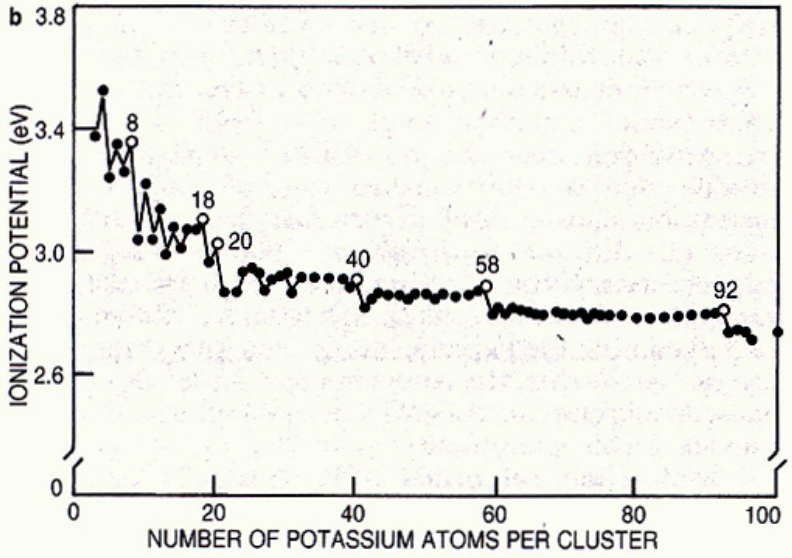

Shell structure: Two views. **a:** Atomic ionization potentials drop abruptly from above 10 eV following the shell closings for the noble gases (He, Ne, Ar and so on). For semiconductors (labeled in blue) the ionization potential is between 8 and 10 eV, while for conductors (red) it is less than 8 eV. It is clear that bulk properties follow from the natures of the corresponding atoms. (Adapted from A. Holden, *The Nature of Solids*, © Columbia U. P., New York, 1965. Reprinted by permission.) **b:** Ionization potentials for clusters of 3 to 100 potassium atoms show behavior analogous to that seen for atoms. The cluster ionization potential drops abruptly following spherical shell closings at $N = 8$, 20, 40 . . . . Features at $N = 26$ and 30 represent spheroidal subshell closings. The work function for bulk potassium metal is 2.4 eV. **Figure 3**

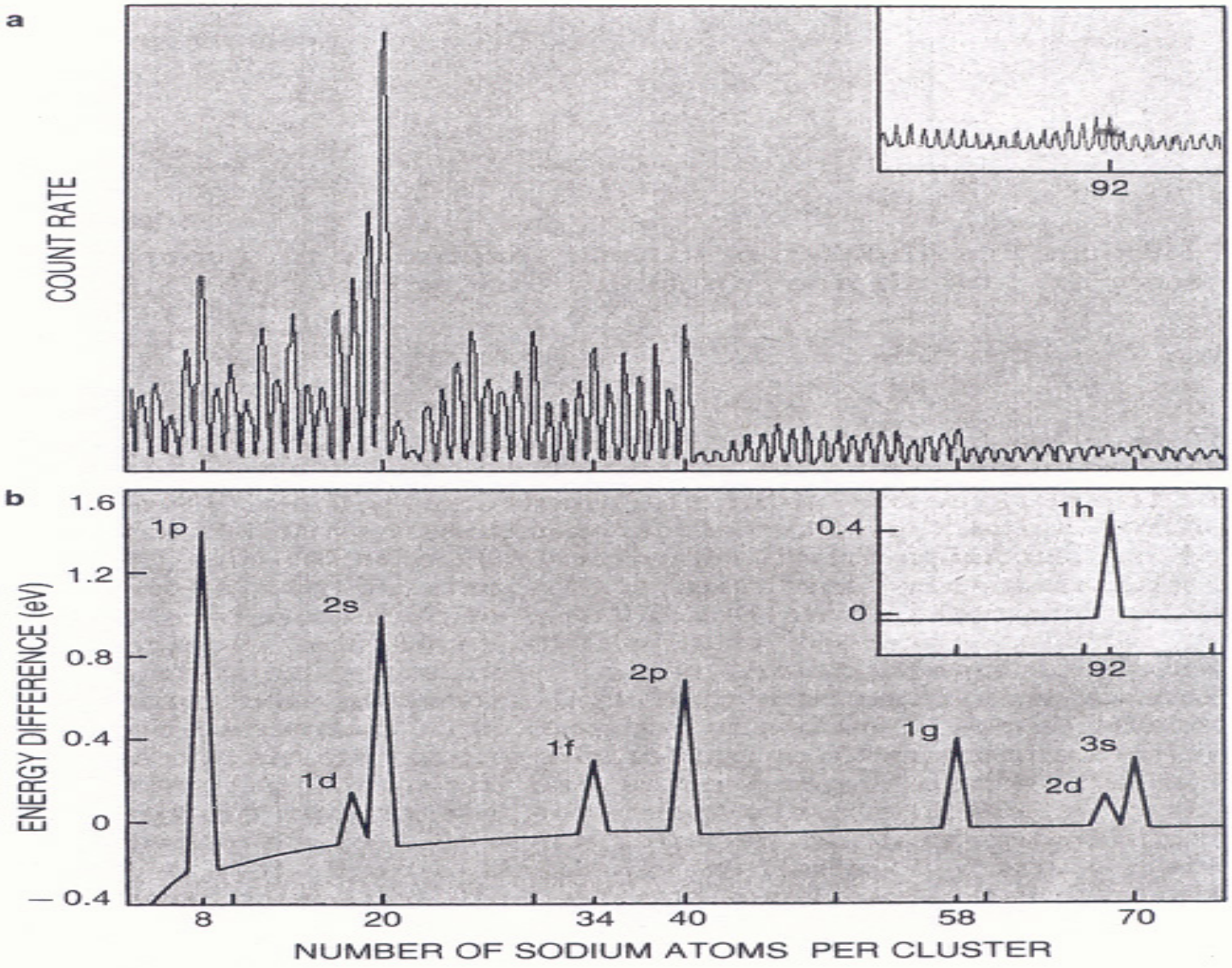
a
COUNT RATE
92
b
ENERGY DIFFERENCE (eV)
1.6
1.2
0.8
0.4
0
−0.4
1p
2s
1d
1f
2p
1g
3s
2d
1h
0.4
0
92
8
20
34
40
58
70
NUMBER OF SODIUM ATOMS PER CLUSTER

Reactivity of nanoclusters

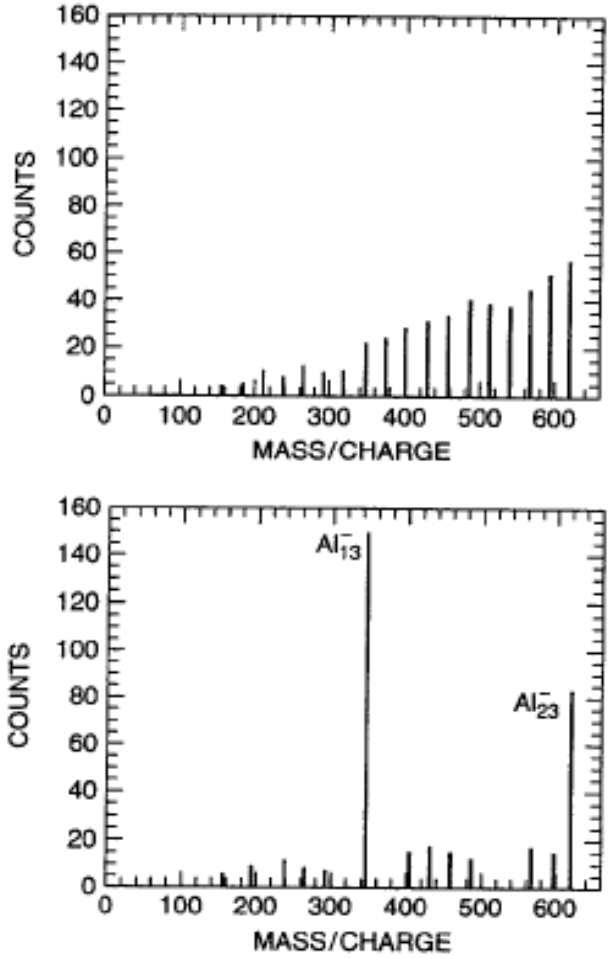

Figure 4.13. Mass spectrum of Al nanoparticles before (top) and after (bottom) exposure to oxygen gas. [Adapted from R. E. Leuchtner et al., *J. Chem. Phys.*, **91**, 2753 (1989).]

Magic clusters

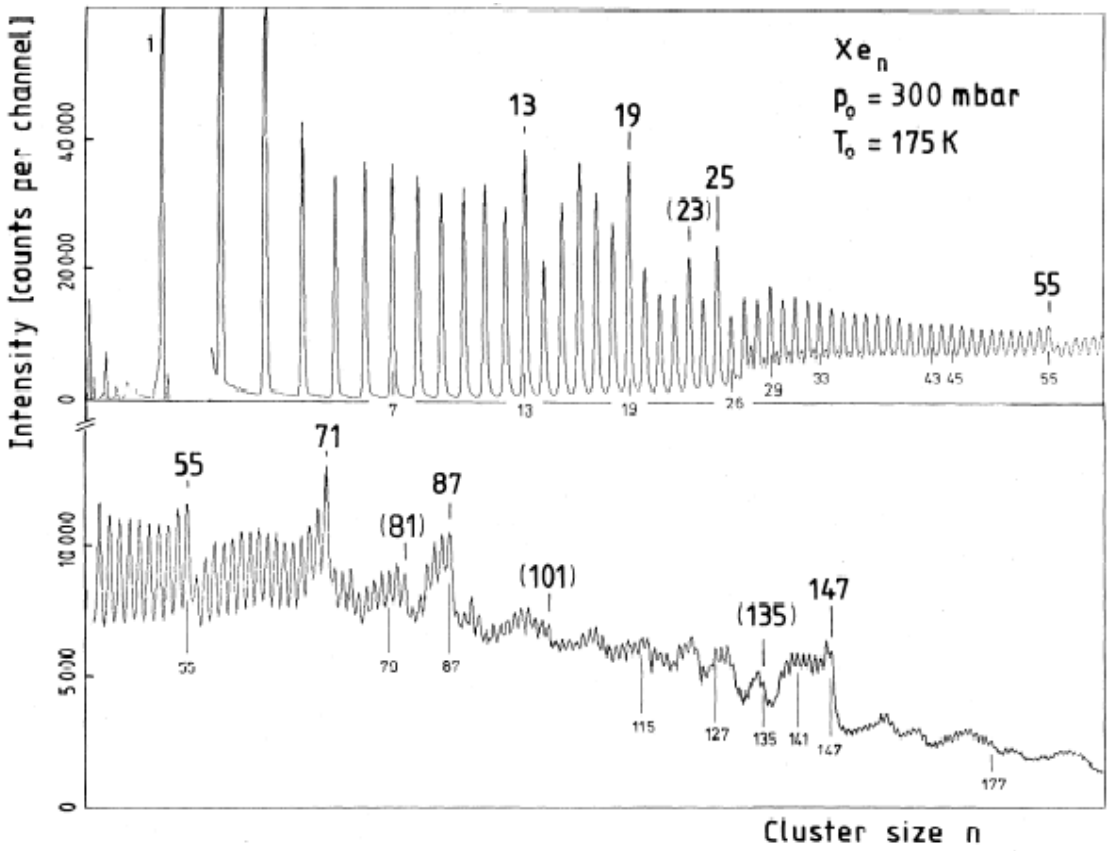

FIG. 1. Mass spectrum of xenon clusters. Observed magic numbers are marked in boldface; brackets are used for numbers with less pronounced effects. Numbers below the curve indicate predictions or distinguished sphere packings.

Mackay icosahedra

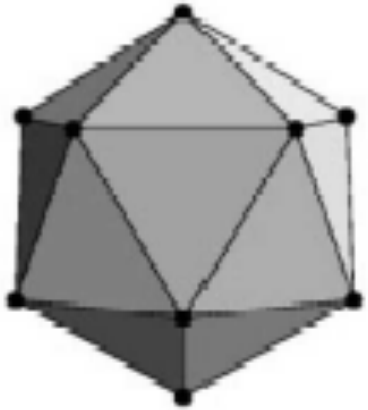

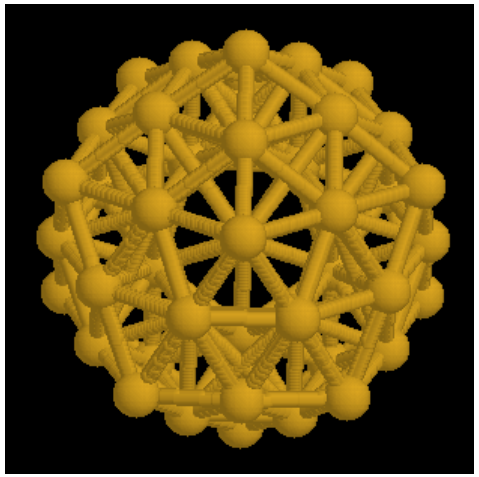

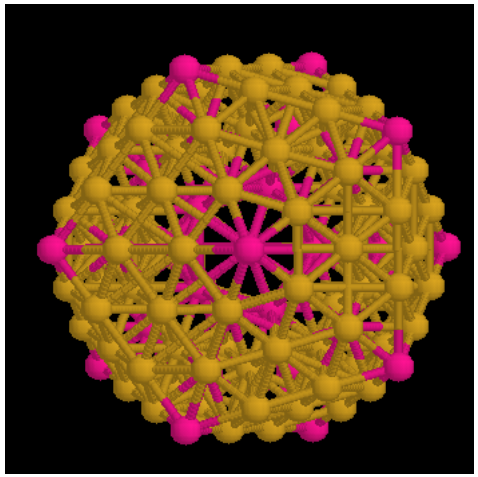

P = 1

P = 2

P = 3

20 fcc(111) faces

Shell model

$$N = 1 + \Sigma\,(10p^2 + 2)$$